

A Stop Operator-Based Prandtl-Ishlinskii Model For Compensation Of Smart Actuator Hysteresis Effects

Omar Aljanaideh

A Thesis
In
The Department
Of
Mechanical and Industrial Engineering

Presented in Partial Fulfillment of the Requirements
for the Degree of Master of Applied Science (mechanical engineering) at
Concordia University
Montreal, Quebec, Canada

November, 2009

© Omar Aljanaideh, 2009



Library and Archives
Canada

Published Heritage
Branch

395 Wellington Street
Ottawa ON K1A 0N4
Canada

Bibliothèque et
Archives Canada

Direction du
Patrimoine de l'édition

395, rue Wellington
Ottawa ON K1A 0N4
Canada

Your file *Votre référence*
ISBN: 978-0-494-71027-2
Our file *Notre référence*
ISBN: 978-0-494-71027-2

NOTICE:

The author has granted a non-exclusive license allowing Library and Archives Canada to reproduce, publish, archive, preserve, conserve, communicate to the public by telecommunication or on the Internet, loan, distribute and sell theses worldwide, for commercial or non-commercial purposes, in microform, paper, electronic and/or any other formats.

The author retains copyright ownership and moral rights in this thesis. Neither the thesis nor substantial extracts from it may be printed or otherwise reproduced without the author's permission.

In compliance with the Canadian Privacy Act some supporting forms may have been removed from this thesis.

While these forms may be included in the document page count, their removal does not represent any loss of content from the thesis.

AVIS:

L'auteur a accordé une licence non exclusive permettant à la Bibliothèque et Archives Canada de reproduire, publier, archiver, sauvegarder, conserver, transmettre au public par télécommunication ou par l'Internet, prêter, distribuer et vendre des thèses partout dans le monde, à des fins commerciales ou autres, sur support microforme, papier, électronique et/ou autres formats.

L'auteur conserve la propriété du droit d'auteur et des droits moraux qui protègent cette thèse. Ni la thèse ni des extraits substantiels de celle-ci ne doivent être imprimés ou autrement reproduits sans son autorisation.

Conformément à la loi canadienne sur la protection de la vie privée, quelques formulaires secondaires ont été enlevés de cette thèse.

Bien que ces formulaires aient inclus dans la pagination, il n'y aura aucun contenu manquant.


Canada

Abstract

A Stop Operator-Based Prandtl-Ishlinskii Model For Compensation Of Smart Actuator Hysteresis Effects

Omar Aljanaideh

The positioning and tracking performance of smart materials actuators is strongly limited due to the presence of hysteresis nonlinearity. The hysteresis of smart actuators, employed in micro-positioning tasks, is known to cause oscillations in the open-loop system's responses, and poor tracking performance and potential instabilities of the close-loop system. Considerable efforts are thus being made continuously to seek effective compensation of hysteresis effects in real-time applications. In this dissertation research, a stop operator-based-Prandtl-Ishlinskii model (SOPI) is proposed as a feedforward compensator for the hysteresis nonlinearities in smart actuators. The complementary properties of the proposed stop operator-based model in relation to the most widely used play operator-based Prandtl-Ishlinskii model are illustrated and applied to realize the desired compensation. It is shown that the stop operator-based model yields hysteresis loops in the clockwise direction, opposite to that of the piezoceramic micro-positioning actuators. It is further proven that the stop operator-based model exhibits concave initial loading behavior, while the play operator-based model, used to characterize the hysteresis behavior, follows a convex initial loading relation between the output and the input. On the basis of these complementary properties, it is hypothesized that a stop operator-based Prandtl-Ishlinskii model may serve as an effective compensator for known hysteresis nonlinearity that is described by a play operator-based model. The proposed stop operator-based model is subsequently implemented as a feedforward compensator in

conjunction with the play operator-based model describing a known hysteresis nonlinearity. The effectiveness of the proposed compensator is demonstrated through simulation and experimental results attained with a piezoceramic micro-positioning stage. Both the simulation and the experimental results show that the proposed stop operator-based model can serve as an effective feedforward hysteresis compensator. A methodology for identifying the stop operator-based model parameters is proposed using those of a known play operator hysteresis model. Relations between the stop and play operator based-model parameters are also derived in the order to facilitate parameter identification. Furthermore, the relation between the stop operator based Prandtl-Ishlinskii model and the inverse Prandtl-Ishlinskii model, which has been proven effective hysteresis compensator, is demonstrated.

Acknowledgments

I am sincerely grateful to my supervisors, Prof. S. Rakheja and Prof. C. Y. Su for their constant guidance and support throughout my thesis work. I would like to thank my parents who have been encouraging and supporting me in my whole life.

Table of Contents

Abstract	ii
List of Figures.....	viii
List of Tables	xi
Chapter 1: Introduction and literature review	1
1.1 Introduction.....	1
1.2 Literature review	3
1.2.1 Hysteresis nonlinearities of smart material actuators.....	4
1.2.2 Hysteresis models.....	8
1.2.3 Hysteresis compensation	14
1.3 Scope and objectives.....	18
1.4 Organization of the thesis	20
Chapter 2: Play and Stop Operator based Prandtl-Ishlinskii Models.....	21
2.1 Introduction.....	21
2.2 Play operator based Prandtl-Ishlinskii (POPI) model.....	22
2.2.1 Play operator.....	22
2.2.2 Play operator based Prandtl-Ishlinskii (POPI) model	25
2.3 Stop operator based Prandtl-Ishlinskii (SOPI) model.....	28
2.3.1 Stop operator	28
2.3.2 Stop operator-based Prandtl-Ishlinskii (SOPI) model.....	30
2.4 Relationship between the play and stop operators.....	32
2.5 Model formulation using shape function	33
2.6 Summary.....	38

Chapter 3: Hysteresis Modeling of a Piezoceramic Actuator	39
3.1 Introduction.....	39
3.2 Experimental characterization of hysteresis of a Piezoceramic actuator	40
3.2.1 Experimental results.....	41
3.2.2 Modeling hysteresis nonlinearities of the piezoceramic actuator using the Prandtl-Ishlinskii model	46
3.3 Model validation	48
3.4 Summary.....	54
Chapter 4: Compensation of Hysteresis Nonlinearities of a Piezoceramic Actuator.....	55
4.1 Introduction.....	55
4.2 Compensation methodology	56
4.3 Hysteresis compensation effectiveness SOPI model	58
4.3.1 Hysteresis compensation using SOPI model with parameters identical to that of the POPI model.....	59
4.3.2 Hysteresis compensation effectiveness of the identified SOPI model.....	60
4.4 Experimental verifications.....	67
4.5 Relations between the SOPI and POPI models.....	70
4.5.1 Relations between the SOPI and POPI models	72
4.5.2 Comparison of the inverse of POPI and SOPI models.....	75
4.6 Summary.....	78
Chapter 5: Major Conclusions and Major Contributions	79
5.1 Major contributions.....	79
5.2 Major conclusions.....	80
5.3 Recommendations for future work	81

References.....	83
Appendix A.....	89

List of Figures

Figure 1.1: Measured hysteresis properties of ferromagnetic materials [6].	5
Figure 1.2: Output-input hysteresis of a magnetostrictive actuator illustrating asymmetry [12].	7
Figure 1.3: The minor and major hysteresis properties of a SMA actuator illustrating output saturation [42].	7
Figure 1.4: Preisach hysteresis operator.	10
Figure 1.5: Krasnosel'skii-Pokrovskii operator.	13
Figure 1.6: Open loop inverse control system.	16
Figure 2.1: A gear mechanism illustrating the play operator behavior.	23
Figure 2.2: Input-output relationship of the play operator.	24
Figure 2.3: (a) Input-output relations of the play operators with different threshold values; (b) Variation in the density function with threshold r and ;(c) the output-input characteristics of the play operator based Prandtl-Ishlinskii (POPI) model under $v(t) = 12\sin(4\pi t)$	27
Figure 2.4: Stop operator.	28
Figure 2.5: (a) Input-output relations of the stop operator with different threshold values; (b) variation in the density function with the threshold s ; and(c) Input-output characteristics of the stop operator based Prandtl-Ishlinskii (SOPI) model based under $v(t) = 4\sin(2\pi t)$	32
Figure 2.6: Input-output characteristics of initial loading curve ψ_f (2.25).	37
Figure 2.7: Input-output characteristics of initial loading curve ψ_e (2.19).	37
Figure 3.1: A schematic representation of the experimental setup.	42

- Figure 3.2: Time histories of the input voltage and output displacement responses of the piezoceramic actuator under different harmonic inputs ($\text{---}\Delta\text{---}$, output displacement; --- , input voltage): (a) $v(t)=40\sin(2\pi t)$; (b) $v(t)=40\sin(10\pi t)$; and (c) $v(t)=5\sin(\pi t)+35\sin(2\pi t)$ 43
- Figure 3.3: Measured input-output characteristics of the piezoceramic actuator under different sinusoidal inputs: (a) $v(t)=40\sin(2\pi t)$; (b) $v(t)=40\sin(10\pi t)$; and (c) $v(t)=5\sin(\pi t)+35\sin(2\pi t)$ 44
- Figure 3.4: Time histories of percent errors in the output of the piezoceramic actuator due to the hysteresis nonlinearities under different inputs: (a) $v(t)=40\sin(2\pi t)$; (b) $v(t)=40\sin(10\pi t)$; and (c) $v(t)=5\sin(\pi t)+35\sin(2\pi t)$ 45
- Figure 3.5: (a) Input-output characteristics of the play operators with different threshold values; and (b) Variations in the density function with the thresholds. 49
- Figure 3.6: Comparisons between the measured displacement responses with the results derived from the Prandtl-Ishlinskii model under different sinusoidal inputs: (a) $v(t)=40\sin(2\pi t)$; (b) $v(t)=40\sin(10\pi t)$; and (c) $v(t)=5\sin(\pi t)+35\sin(2\pi t)$. ($\text{---}\Delta\text{---}$, measured; --- , model). 51
- Figure 3.7: Comparisons of time histories of measured displacement responses and the outputs of the play operator-based Prandtl-Ishlinskii model under different sinusoidal inputs: (a) $v(t)=40\sin(2\pi t)$ (b); $v(t)=40\sin(10\pi t)$; and (c) $v(t)=5\sin(\pi t)+35\sin(2\pi t)$ ($\text{---}\Delta\text{---}$, measured; --- , model). 52
- Figure 3.8: Time-histories of percent displacement error under the three inputs: (a) $v(t)=40\sin(2\pi t)$; (b) $v(t)=40\sin(10\pi t)$; and (c) $v(t)=5\sin(\pi t)+35\sin(2\pi t)$ 53
- Figure 4.1: Illustration of hysteresis compensation via stop operator based Prandtl-Ishlinskii model. 58
- Figure 4.2: Input-output characteristics of: (a) the SOPI model; and (b) the POPI model under $v(t)=10\sin(2\pi t)$ 60
- Figure 4.3: Compensation of hysteresis nonlinearities described by a POPI model output $\Phi[v](t)$ presented in Figure 4.2(b) using the SOPI model $\Gamma[v](t)$ presented in Figure 4.2(a). 61
- Figure 4.4: The output-input characterization of the SOPI model Γ_c , identified from the known POPI model Φ , and the compensated output under input $v(t)=10\sin(2\pi t)$ 63

- Figure 4.5: The time history of percent error in actuator displacement response with and without the SOPI model feedforward compensator: without feedforward compensator (dotted line); with arbitrary SOPI model Γ compensator (dashed line); with identified SOPI model Γ_c compensator (solid line). 63
- Figure 4.6: The output-input characterization of the SOPI model Γ_c , identified from the known POPI model Φ , and the compensated output under different inputs (a) $v(t)=40\sin(2\pi t)$; (b) $v(t)=40\sin(10\pi t)$; (c) $v(t)=15\sin(\pi t)+25\sin(2\pi t)$; (d) $v(t)=5\sin(\pi t)+35\sin(2\pi t)$; and (e) $v(t)=20\sin(\pi t)+20\sin(4\pi t)$ 67
- Figure 4.7: Experimental setup for compensation of hysteresis nonlinearities of the piezoceramic actuator using stop operator-based Prandtl-Ishlinskii (SOPI) model as a feed forward compensator. 68
- Figure 4.8: Input-output characteristics of the piezoceramic stage with SOPI model under the input: (a) $v(t)=40\sin(2\pi t)$; (b) $v(t)=40\sin(10\pi t)$; and (c) $v(t)=5\sin(\pi t)+35\sin(2\pi t)$ 69
- Figure 4.9: Time histories of the percent position error under different sinusoidal inputs with and without SOPI model compensator: (a) $v(t)=40\sin(2\pi t)$; (b) $v(t)=40\sin(10\pi t)$; and (c) $v(t)=5\sin(\pi t)+35\sin(2\pi t)$. (Solid line, with feedforward SOPI model compensator- simulation); (dashed line, with feedforward SOPI model compensator- experimentally); and (dotted line, without feedforward SOPI model compensator- experimentally). 71
- Figure 4.10: Variation in (a) the thresholds of the SOPI model with those of POPI model; and (b) the density function values of the SOPI model and those of the POPI model..... 72
- Figure 4.12: The time history of percent error of compensation error with SOPI models $\bar{\Gamma}$ and Γ_c . (——, with $\bar{\Gamma}$ model; — Δ — with Γ_c model). 74
- Figure 4.11: Compensation of hysteresis nonlinearities described by a POPI model output $\Phi[v]$ presented in (b) and (e), using: (a) the SOPI model output $\bar{\Gamma}$ presented in (a), and the proposed SOPI model Γ_c model presented in (d). 74
- Figure 4.13: Comparison of the input-output responses of the inverse POPI Φ^{-1} and SOPI models Γ_c under a sinusoidal input: $v(t)=40\sin(2\pi t)$, (——, inverse POPI model Φ^{-1} ; — Δ —, SOPI model Γ_c). 77
- Figure 4.14: Time-history of the percent error between the inverse of POPI and the SOPI models output. 77

List of Tables

Table 3.1: The peak percent positioning error of the piezoceramic actuator.....	46
Table 3.2: Identified parameters of the Prandtl-Ishlinskii model based on the play operator.	48
Table 3.3: Variations in the values of the thresholds and density function of the play operator based- Prandtl-Ishlinskii model.....	48
Table 3.4: Summary of errors between the measured responses and the outputs of the play operator based Prandtl-Ishlinskii under the inputs considered.	50
Table 4.1: Parameters of the Prandtl-Ishlinskii model based on the stop operator (SOPI) identified through solution of the minimization problem.	65
Table 4.2: The values of the thresholds and density function of the stop operator based Prandtl-Ishlinskii model.....	65
Table 4.3: Peak position error (peak percent error).	71
Table 4.4: The thresholds and the density function values of SOPI models $\bar{\Gamma}$ and Γ_c	73

Chapter 1

Introduction and literature review

1.1 Introduction

Although classical actuators (electromagnetic, hydraulic and pneumatic) are widely used in the industry, new technologies based on physically different principles have emerged during the past two decades for applications requiring miniaturization in size, fast response and high resolution. Smart materials have been employed to meet these demands for micro-positioning and actuation. Such materials are able to change their physical properties such as stiffness in response to external effects like stress or electric fields. Piezoceramic materials are among the most common materials which are widely being used in micro-actuators. Such smart materials actuators, however, exhibit strong nonlinearities between the input and the output associated with material hysteresis and saturation.

Hysteresis is invariably observed in smart materials due to deformation, in magnetism, and even in biological systems [1,2,3]. Piezoceramic actuators used in micropositioning and vibration control exhibit hysteresis nonlinearities between the input voltage and the output displacement [4,5,6,7]. These nonlinearities can be presented by counter-clockwise hysteresis loops, and are known to cause oscillations in the responses of the open-loop systems, and poor tracking performance and potential instabilities in the closed-loop systems [8]. Considerable efforts have thus been made towards design of controllers for compensation of hysteresis effects. The majority of the reported compensation methods could be classified in two broad categories: model-based [9] and

inverse model-based control methods [8,10,12,13]. The model-based hysteresis compensation methods employ hysteresis models of the actuator to design nonlinear controllers such as robust adaptive and energy-based control systems [11,14].

The inverse model-based hysteresis compensation methods employ a cascade of a hysteresis model and its inverse together with a controller to compensate for the hysteresis effects [4]. Such methods can yield more effective compensation of hysteresis effects in an efficient manner compared to the model-based compensation methods. Furthermore, the inverse-model based methods can compensate for broad range of hysteresis nonlinearity. These methods, however, necessitate formulation of an inverse of the hysteresis model, which is often a challenging task. Considerable efforts have been made in deriving either numerical or analytical inverse of the operator-based phenomenological hysteresis models, which is implemented as a feedforward hysteresis compensator in conjunction with a relatively simpler controller.

The reported studies on both the model and the inverse model-based compensation methods have mostly employed operator-based phenomenological hysteresis models such as Preisach [14] and Prandtl-Ishlinskii [11] models. The majority of the operator-based hysteresis models, with the exception of the Prandtl-Ishlinskii model, however, are not analytically invertible. Consequently, a number of studies have employed numerically-derived inversions of the Preisach and Krasnosel'skii-Pokrovskii models [4,10,15,16], which may be considered valid in the vicinity of conditions or ranges used in defining the inverse.

Alternatively, the Prandtl-Ishlinskii hysteresis model [17] offers a unique property associated with its play and stop operators that may be explored to achieve hysteresis

compensation in a more efficient manner. The stop operator model exhibits complementary property in the relation to the direction of hysteresis loops of the play operator [17]. In this dissertation, it is hypothesized that the stop operator-based Prandtl-Ishlinskii (SOPI) model could serve as an effective feedforward compensator to compensate the hysteresis nonlinearity described by the play operator-based Prandtl-Ishlinskii (POPI) model, although a (SOPI) model cannot characterize the hysteresis of a smart actuator. This dissertation research presents the formulation of a stop-operator based Prandtl-Ishlinskii model to achieve hysteresis compensation. Essential relationships between the play and stop operator-based models are formulated to facilitate identification of the proposed stop operator-based model from the known hysteresis model. The effectiveness of the proposed stop operator-based compensator is demonstrated through various simulation examples and experiments on a piezoceramic actuator.

1.2 Literature review

Compensation of hysteresis in smart actuator systems involves: characterization and modeling of hysteresis in smart actuators, and developments in compensation algorithms and controllers. The reported relevant studies in each of these domains are reviewed to build essential background knowledge and to formulate the scope of this dissertation research. The reviewed studies are systematically grouped under different relevant topics and summarized in the following subsections.

1.2.1 HYSTERESIS NONLINEARITIES OF SMART MATERIAL ACTUATORS

The hysteresis properties of different materials and smart actuators have been characterized through experimental means in order to enhance an understanding of the essential properties and to seek methods for modeling this phenomenon. Although the experimentally measured hysteresis properties of ferromagnetic materials have been extensively reported [4,18], the properties of piezoceramic actuators have been reported in a few recent studies [3,19]. The ferromagnetic materials and smart actuators generally exhibit major and minor loops in the output-input characteristics together with output saturation nonlinearity. Figure 1.1 illustrates typical hysteresis nonlinearity of ferromagnetic materials between the applied electric field and the response flux density [18]. The piezoceramic and shape memory alloy (SMA) actuators also exhibit similar hysteresis nonlinearity. The essential hysteresis properties can be generally summarized as follows:

1. The relation between the output and the input is causal, and the output depends on the past and current value of the input;
2. The output tends to saturate as the input exceeds certain limit;
3. The output is monotone continuous and it increases or decreases with increasing or decreasing input;
4. Major loops in the output-input characteristics are obtained when the input is increased to a maximum value, and decreased to a minimum value. The hysteresis minor loops are obtained under relatively small variations in the input;
5. The width of the hysteresis loop is referred to the coercivity of the material, which increases as the amplitude of the input is increased. The coercivity generally approaches its maximum value near zero input.

Many studies have experimentally characterized the hysteresis in smart material actuators in order to enhance an understanding of the hysteresis properties, particular the effects of various contributing factors such as the rate and the magnitude of the input. These studies have reported hysteresis properties of piezoceramic, shape memory alloy (SMA) and magnetostrictive actuators [14,21].

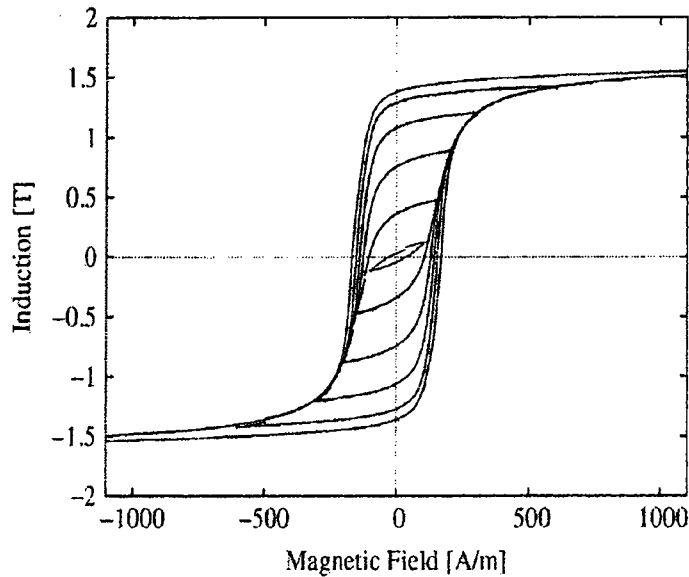


Figure 1.1: Measured hysteresis properties of a ferromagnetic material [18].

The characterizations of hysteresis properties of piezoceramic actuators through measurements and modeling have been the focus on many studies due to their various potential applications in micro-positioning tasks. These studies show that piezoceramic actuators exhibit strong hysteresis effects between the input voltage and the measured output displacement, while the hysteresis loops are generally symmetric about the input and the output [3]. It has also been shown that such hysteresis is known to cause inaccuracy and oscillations in the system response, and potential instability of the closed loops system [8].

Ge and Jouaneh [3] performed measurements to characterize the hysteresis properties of a piezoceramic actuator. The actuator used in the study provided a nominal displacement of 20 μm under an excitation of 1000 V and a capacitive sensor with a resolution of 2.5 nm was used to measure the displacement response of the actuator. The measurements were performed under sinusoidal voltage input of amplitude of 800 V at two distinct frequencies (0.1 and 100 Hz). The study concluded that both the excitations yield similar hysteresis suggesting negligible effect of the rate of input. In similar manner, Hu and Ben Mrad [20] measured the hysteresis of a piezoceramic actuator (nominal displacement = 3000 nm) under an input voltage of 100 V at different frequencies. The study concluded that the width of the measured voltage-displacement loop was nearly 15% of the maximum actuator expansion under a very low frequency input, and increased under higher frequency inputs. Yu et al. [19] measured the hysteresis properties of piezoceramic patches and SMA coupled with a cantilever beam. The study was performed to characterize the minor hysteresis loops and wiping out properties of the beam coupled with the actuator. The results showed strong hysteresis nonlinearities and the wiping out property.

The hysteresis properties of magnetostrictive actuators and shape memory alloys (SMA) have also been investigated in many studies [10,21,22]. Unlike the piezoceramic material actuators, the magnetostrictive actuators, consisting of ferromagnetic materials such as Terfenol-D, exhibit asymmetric hysteresis loops between the input and the output, as shown in Figure 1.2. Shape memory alloys (SMA) such as nickel-titanium, exhibit a saturation of the output displacement with increasing input temperature, as shown in Figure 1.3. The hysteresis properties of SMA have been measured by varying

the input temperature in the materials and the displacement output. These materials show capability to recover strain (up to 10%) without permanent deformation [14].

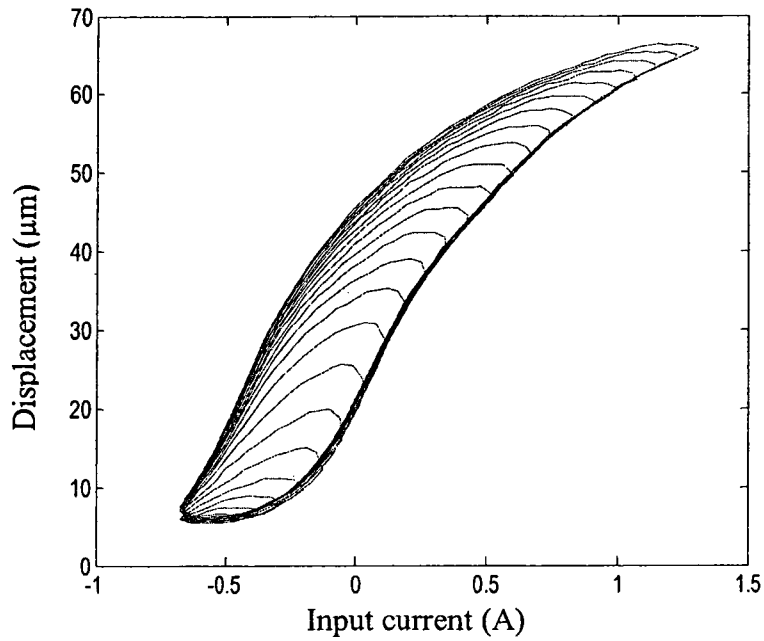


Figure 1.2: Output-input hysteresis of a magnetostrictive actuator illustrating asymmetry [21].

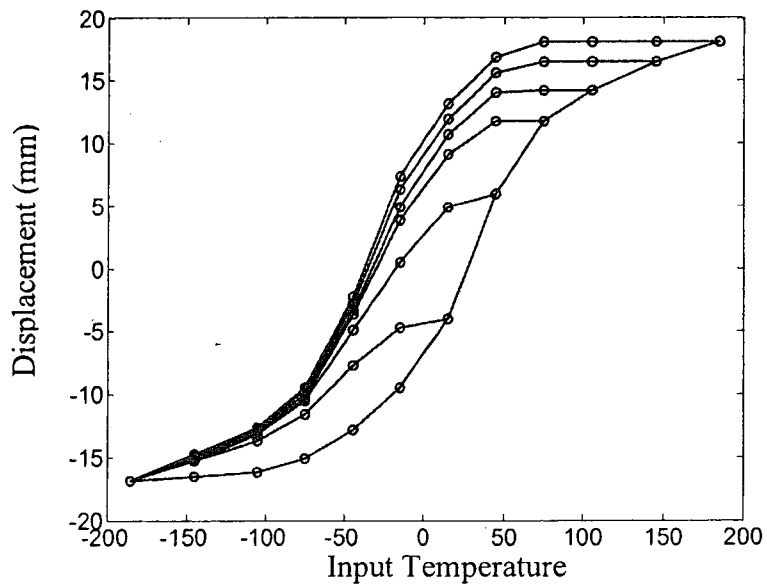


Figure 1.3: The minor and major hysteresis properties of a SMA actuator illustrating output saturation [14].

1.2.2 HYSTERESIS MODELS

A large number of analytical models have been proposed to characterize the hysteresis properties of smart actuators. The primary goal of these models is to predict the hysteresis behavior of materials and smart actuators in order to study the effects of hysteresis and facilitate the design of controllers and hysteresis compensation. These models may be generally classified into physics based models [4,9,23] and phenomenological models [17,18,24]. The physics based models are built on the physical measures such as energy or displacement. The physics based models generally require knowledge of the physical system and the phenomenon which may be quite complex for many materials considering the strong hysteresis nonlinearity. Moreover, the physics-based models are considered applicable for a particular material or actuator, while their inverse may not be attainable for hysteresis compensation [4,23]. The phenomenological models, on the other hand characterize the hysteresis properties on the basis of known input-output characteristics. The phenomenological models can be further classified into differential equation-based phenomenological models such as: Duhem model [25] and Bouc-Wen model [25]; and the operator-based hysteresis models such as: Preisach model [18], Prandtl-Ishlinskii model [17] and Krasnosel'skii-Pokrovskii model [28]. The differential equation-based models comprise nonlinear differential equation for describing the input-output relations. Such models, however, exhibit several limitations for control system design applications [25], and pose considerable challenges in parameters identification. Moreover, these models are not invertible and cannot be applied for effective hysteresis compensation [25]. The operator based Preisach and Krasnosel'skii-Pokrovskii models have been most widely used to characterize the

hysteresis behavior of smart actuators. These models are briefly described below, while the Prandtl-Ishlinskii model is described in greater details in chapter 2.

Preisach model

The first attempt to characterize hysteresis was carried out by Preisach in 1939. The Preisach model [18] has been widely used in modeling a wide range of hysteresis phenomenon in electromagnetic materials and smart actuators. In [18], Mayergoyz describes the mathematical properties and formulation of the Preisach model. The Preisach model employs an infinite set of relay operators $\gamma_{\alpha\beta}$, while the output of the model is derived from a superposition of a set of the relay operators. For a given input $v(t) \in C_m [0, T]$, the output of the relay operator $\gamma_{\alpha\beta}[v](t)$ is given by:

$$\gamma_{\alpha\beta}[v](t) = \begin{cases} +1 & \text{if } v(t) \geq \alpha \\ -1 & \text{if } v(t) \leq \beta \\ \gamma_{\alpha\beta}[v](0) & \text{if } v(t) < \alpha \ \& \ v(t) > \beta \end{cases} \quad (1.1)$$

where $v(t)$ is the input, and the constants α and β define the switching or the threshold values of the input corresponding to upward and downward shifting of the output, respectively, as shown in Figure 1.4.

In the above formulation $\gamma_{\alpha\beta}[v](0)$ is given by:

$$\gamma_{\alpha\beta}[v](0) = \begin{cases} +1 & \text{if } v(0) \geq \alpha \\ -1 & \text{if } v(0) \leq \beta \\ \lambda & \text{if } v(0) < \alpha \ \& \ v(0) > \beta \end{cases} \quad (1.2)$$

The above operator forms the building block for the Preisach model, where the output of the operator is either +1 or -1 depending on the value of the current input. The

output switches from -1 to +1 when the current input is larger than α , and from +1 to -1 when the current input is less than β . The operator thus exhibits strong discontinuities near $v(t)=\alpha$ and $v(t)=\beta$, while the output is limited to either 1 or -1.

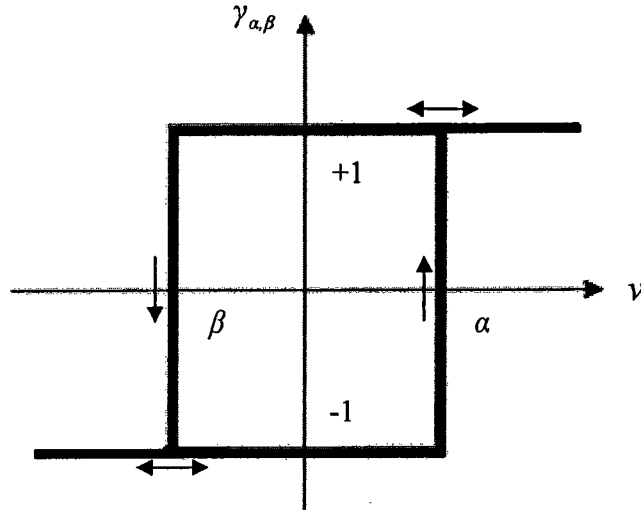


Figure 1.4: Preisach hysteresis operator.

The Preisach hysteresis model is formulated upon integration of the operators $\gamma_{\alpha\beta}$ and expressed as:

$$y(t) = \iint_{\alpha \geq \beta} \mu(\alpha, \beta) \gamma_{\alpha\beta}[v](t) d\alpha d\beta \quad (1.3)$$

where $\mu(\alpha, \beta)$ represents the weightings of the relay operators also known as the density function, which are generally identified from the measured data of a particular material or actuator. The function $\mu(\alpha, \beta)$ is integrable and positive.

In [18], Mayergoyz further defines two essential properties of the Preisach model: (i) the wiping out property; and (ii) the congruent minor loop property. These are the necessary and sufficient conditions for existence of a Preisach model. The wiping out

property states that extrema of the input can remove the effects of a previous extrema, essentially the memory of the model will be wiped out. The congruent minor-loop property states that at any point on the minor loop, the output variation from the previous extremum will be identical for both inputs and the minor loops will have the same shape. Furthermore, the two minor loops are considered to be equivalent only if they are generated by identical monotonically varying inputs.

The reported studies have proposed different forms of the classical Preisach model for characterizing hysteresis in various systems such as piezoceramic [3], magneto-restrictive [20,21,27,29] and SMA actuators [14,30,31]. Ge and Jouaneh [3] modified the classic Preisach operator with output threshold of either '-1' or '+1' to an alternate Preisach operator with threshold or switching values of '0' or '+1' considering the unidirectional dipoles polarization of the piezoceramic materials. A few studies have proposed alternate density functions to accurately characterize the hysteresis behavior of different actuators [2,18,19]. For instance, Hughes and Wen [2] applied the Preisach model for characterizing the hysteresis of piezoceramic and SMA actuators by integrating a density function in the form of a second-order polynomial. The study verified wiping out and the minor loops properties for both the actuators by applying a decaying sinusoidal input. A few studies have also proposed dynamic density functions in the Preisach model to describe rate dependent hysteresis effects of smart actuators [10,19]. The validity of such models has been demonstrated by illustrating good agreements between the measured hysteresis properties and the model responses to inputs at different frequencies [19,20].

Krasnosel'skii-Pokrovskii model

The Krasnosel'skii-Pokrovskii operator is a hysteresis operator that is derived from the Preisach hysteresis operator [16,24,28]. This operator is constructed from two different functions that are bounded by two piecewise Lipschitz continuous functions. A ridge function $\delta(v)$ is used to formulate the Krasnosel'skii-Pokrovskii operator, which is given by:

$$\delta(v) = \begin{cases} -1 & \text{for } v(t) < 0 \\ -1 + \frac{2v(t)}{a} & \text{for } 0 \leq v(t) \leq a \\ 1 & \text{for } v(t) > a \end{cases} \quad (1.4)$$

where $a > 0$ is a constant, as shown in the output-input characteristics of the operator in Figure 1.5. For a given input $v(t) \in C[0, T]$, the output of the Krasnosel'skii-Pokrovskii operator is expressed as:

$$M(t) = \begin{cases} \max(M(t_-), \delta(v(t) - \alpha)) & \text{for } v(t) > v(t_-) \\ \min(M(t_-), \delta(v(t) - \beta)) & \text{for } v(t) < v(t_-) \\ M(t_-) & \text{for } v(t) = v(t_-) \end{cases} \quad (1.5)$$

where $M(t)$ is the output, and α and β are constants similar to those defined for the Preisach relay operator. The Krasnosel'skii-Pokrovskii operator maps $C[0, T]$ to $C[0, T]$ [28]. Unlike the Preisach operator, the K-P operator exhibits finite slope as seen in Figure 1.5, which suggests that the operator is Lipschitz continuous. The output of the Krasnosel'skii-Pokrovskii model, $\Psi[v](t)$, is expressed by [28]:

$$\Psi[v](t) = \iint_{\alpha \geq \beta} \rho(\alpha, \beta) M[v](t) d\alpha d\beta \quad (1.6)$$

where $\rho(\alpha, \beta)$ is an integrable positive density function.

Banks et al. [32] investigated the properties of the Krasnosel'skii-Pokrovskii model for characterizing hysteresis nonlinearities in smart actuators, particularly SMA actuators. Another study implemented Krasnosel'skii-Pokrovskii operators instead of the Preisach relay operators in the Preisach model for characterizing hysteresis nonlinearities of a piezoceramic actuator [16].

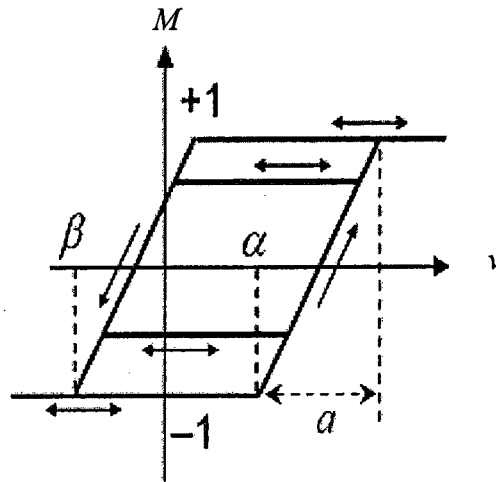


Figure 1.5: Krasnosel'skii-Pokrovskii operator.

Prandtl-Ishlinskii model

The Prandtl-Ishlinskii model [17] is constructed using either play or stop operators. Unlike the discontinuous relay operators in the Preisach model, the play and stop operators are continuous hysteresis operators, which are characterized by an input v and the threshold value. The hysteresis properties of smart actuators have been invariably characterized using integration of the play operators in the Prandtl-Ishlinskii model [12,39], while the application of the stop operator has been limited to hysteresis of materials in a few earlier studies [17]. Ge [33] investigated the play operator under different input signals (sinusoidal and arbitrary) at low frequencies, applied a linearizing algorithm to compensate for play operator nonlinearity in tracking control simulation.

Janocha and Kuhnen [35] characterize the hysteresis of piezoceramic actuator using play operator based Prandtl-Ishlinskii model and compensated the hysteresis effects using inverse Prandtl-Ishlinskii model, which was constructed numerically, Krejci and Kuhnen [12] applied the Prandtl-Ishlinskii model and an analytical inverse of the Prandtl-Ishlinskii model to characterize and compensate hysteresis nonlinearities of a piezoceramic actuator. While the stop operator has been proposed in the literature to characterize elastic-plastic behavior in continuum mechanics [17], the stop operator based Prandtl-Ishlinskii model could not be used in characterizing hysteresis in smart actuators since it exhibits clockwise hysteresis loops in the input-output curves. Alternatively, this model could be used as a feedforward compensator in open loop system to compensate for hysteresis nonlinearities. The Prandtl-Ishlinskii models with play and stop operators are described in the subsequent chapter.

1.2.3 HYSTERESIS COMPENSATION

The hysteresis nonlinearities in smart actuators have been associated with oscillations and poor tracking performance of micro-positioning devices employing smart actuators. Numerous efforts have thus been made to design controllers for compensating the nonlinear hysteresis effects in smart actuators and to enhance the tracking performance [7,10,12,22]. Although a number of controller syntheses have been proposed to reduce the error due to hysteresis effects in smart actuators, continued efforts are being made to seek more effective and efficient hysteresis compensation methods. The proposed compensation algorithms could be classified in two broad categories based upon the approach, namely: non-inverse and inverse based methods, which are briefly described below.

Non-inverse based control methods

Compensation of hysteresis nonlinearities has been carried out in many studies without considering the inverse of the hysteresis models, although the hysteresis may be characterized by a hysteresis model. A number of control methods have been proposed to compensate for smart actuators hysteresis such as robust adaptive [11], energy-based [14], and sliding model control systems [36]. In [11], Su et al. proposed an adaptive controller that is employed to control a nonlinear system preceded by unknown Prandtl-Ishlinskii hysteresis nonlinearities. In this study, the proposed controller leading to the desired output and the global stability was presented. Gorbet et al. [14] proposed a control approach based on energy to control a SMA actuator, which showed hysteresis nonlinearities. The study employed the Preisach model, and verified the energy properties and the state space of the model. The minimum energy states were recommended to formulate the controller synthesis and the passivity was established for the relationship between the input and the time rate of the Preisach model output on the basis of the energy. The results demonstrated the effectiveness of the method in compensating the hysteresis of the SMA actuator. Liaw et al. [36] proposed a sliding mode adaptive controller to control the hysteresis of a piezoceramic actuator. The piezoceramic actuator was characterized using an electromechanical, analytically expressed by a second-order differential equation. The study demonstrated that the proposed sliding model controller can effectively compensate for the hysteresis nonlinearities of the piezoceramic actuator.

Inverse model based control methods

The inverse model-based hysteresis compensation methods employ the inverse of the hysteresis model as a feedforward compensator in a cascade arrangement of the hysteresis model and its inverse. These methods are considered to be more effective and convenient for real-time compensation and control [10,12,37]. The inverse model-based compensation, however, necessitates the formulation of the hysteresis model inverse, which is often a challenge task. An open-loop inverse model-based compensation method, shown in Figure 1.6, has been widely proposed in the literature to reduce the effects of hysteresis. In this figure, u is the control input, Π^{-1} is an inverse hysteresis model, Π represents a hysteresis model and v^* is the desired output. This method is pioneered by Tao and Kokotovic [8], and involves the formulation of the inverse model of the hysteretic system. Their study developed a control algorithm to compensate the hysteresis nonlinearities of a system comprising a linear plant preceded by a hysteresis block representing a hysteretic actuator. An adaptive hysteresis inverse compensator was cascaded together with the hysteresis system to mitigate the effects of hysteresis.

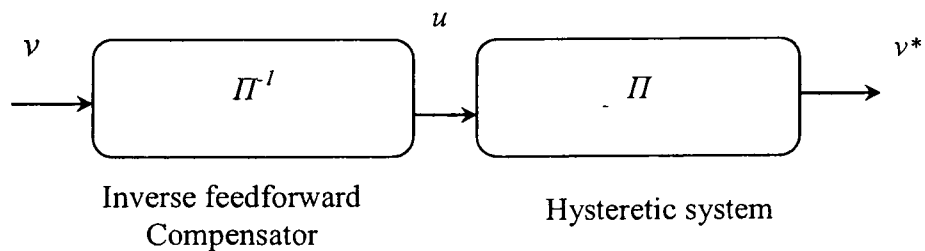


Figure 1.6: Open loop inverse control system.

The implementation of an inverse-model based compensation, however, may involve complexities associated with formulations of the inverse. The Preisach and

Krasnosel'skii-Pokrovskii models are not analytically invertible. Different numerical methods have thus been developed to obtain inversions of these models. Ge and Jouaneh [7] used the inverse Preisach model, desired using a numerical algorithm, as a feedforward compensator coupled with a PID feedback control system to reduce the hysteresis nonlinearities in a piezoceramic actuator. A numerical inverse of the Krasnosel'skii-Pokrovskii model was applied by Galinaitis [16] in an open-loop control system to compensate hysteresis of a piezoceramic actuator. In this study, the compensation of the hysteresis nonlinearities was demonstrated for three different sinusoidal inputs at a frequency of 0.05 Hz. In a similar manner, Song et al. [62] proposed a modified Preisach model to characterize and to compensate the hysteresis nonlinearities in a piezoceramic actuator with PD-lag and PD-lead controllers together with the inverse of the modified model in a closed loop control system. Reduction in the hysteresis nonlinearity was demonstrated experimentally for major and minor hysteresis loops under low excitation frequencies (0.5 Hz). Tan and Baras [10] applied an inverse Preisach model, which was obtained numerically, in an adaptive control system to compensate the hysteresis nonlinearities of a magnetostrictive actuator. Janocha and Kuhnen [35] compensated the hysteresis effects of a piezoceramic actuator using the inverse Prandtl-Ishlinskii model, which was constructed numerically, in an open loop control system.

Unlike the Preisach and Krasnosel'skii-Pokrovskii models, the Prandtl-Ishlinskii model offers a unique advantage, since its inverse can be obtained analytically. Krejci and Kuhnen [12] applied the analytical inverse of the Prandtl-Ishlinskii model as a feedforward compensator for mitigating the hysteresis nonlinearities. A recent study has

proposed a generalized Prandtl-Ishlinskii model and its analytical inverse to compensate for rate dependent and asymmetric hysteresis nonlinearities in a class alls of smart actuators [40]. This model also offers another unique property associated with its play and stop operators that may be explored to achieve hysteresis compensation in a more efficient manner. The Prandtl-Ishlinskii model can be constructed using either the play or stop hysteresis operators, while the reported hysteresis models are invariably based on the play operator, which exhibits counter-clockwise hysteresis loops. These Prandtl-Ishlinskii models have been extensively used to characterize hysteresis properties of piezoceramic actuators, which are symmetric about the input [12,48]. The Prandtl-Ishlinskii model based on the stop operator, on the other hand, exhibits clockwise hysteresis loops, which is attributed to the stop operator [17].

1.3 Scope and objectives

The smart actuators employed in micropositioning applications exhibit oscillations in the response and poor tracking performance, which have been attributed to their strong hysteresis nonlinearities. The compensation of such hysteresis effects through adequate controller designs is thus considered an important task. Although various non-inverse and inverse model based compensation methods have been proposed to effectively compensate for the hysteresis nonlinearity. While the non-inverse model based methods require complex controller design, the vast majority of the inverse model based methods rely on approximate numerical inverse of the hysteresis model. In this dissertation, it is hypothesized that the stop-operator based Prandtl-Ishlinskii model, owing to its complementary property with respect to the classical play-operator based model, could serve as effective hysteresis compensation when applied in a feedforward

manner. Although the Prandtl-Ishlinskii models for characterizing hysteresis nonlinearity of smart actuators have been invariably formulated using the play operator, a few studies on materials hysteresis characterization have employed the stop operator. The stop operator based model exhibits hysteresis loops in the clockwise direction opposite to that of the play operator based model. This complementary property of the stop and play operators may be utilized to achieve hysteresis compensation through implementation of a cascade arrangement of the composition of play operator based hysteresis model with stop-operator based model in an open loop manner. Furthermore, the continuous nature of the Prandtl-Ishlinskii model and availability of its exact inverse could help identify essential relations for identify the parameters of the stop operator based model.

The primary objective of this dissertation research is thus formulated to explore the above stated hypothesis for achieving compensation of hysteresis nonlinearity in smart actuators the specific objectives of the dissertation research are:

- Formulate a stop operator based Prandtl-Ishlinskii model and investigate its properties, particularly the complementary property with the play operator;
- Investigate the hysteresis compensation effectiveness of the stop operator based Prandtl-Ishlinskii model through simulations and in the laboratory for a piezoceramic micro actuators; and
- Formulate relations methodology for identifying the parameters of the stop operator-based model using the known hysteresis of a particular smart actuator.

In this dissertation research, a stop operator based Prandtl-Ishlinskii hysteresis model is formulated on the basis of known hysteresis properties of a smart actuator. For this purpose, the widely-documented play operator based Prandtl-Ishlinskii hysteresis model is

used to characterize the hysteresis of the smart actuator. The well-known play-operator based Prandtl-Ishlinskii model is formulated, thus presented in Chapter 2, where the model parameters are identified using the laboratory-measured data acquired for a piezoceramic actuator. The resulting play operator based model is subsequently applied to develop the stop operator based model for compensation of hysteresis effects.

1.4 Organization of the thesis

This dissertation research is organized in four chapters. Chapter 2 presents the play and stop operator based Prandtl-Ishlinskii models in details, including the mathematical properties and physical behaviors of these operators. The play and stop operator based Prandtl-Ishlinskii models are formulated to investigate their input-output properties and their complementary property. Furthermore, the shape functions are employed for both the models to investigate the behavior of the stop and play operator-based models. In Chapter 3, experimentally-measured hysteresis properties of a piezoceramic actuator are utilized to demonstrate the validity of the play operator based Prandtl-Ishlinskii model for characterizing the hysteresis nonlinearities of the piezoceramic actuator. Chapter 4 presents the formulation of the stop operator based Prandtl-Ishlinskii model and its implementation as a feedforward compensator to compensate the hysteresis effects. The effectiveness of the model is investigated through simulations and also through experiments conducted on a piezoceramic actuator. A methodology to identify the parameters of the stop operator-based model is presented and the relationships between the parameters of the stop-operator and the inverse model parameters are explored. The major conclusions and the recommendations for further works are finally summarized in chapter 5.

Chapter 2

Play and Stop Operator Based Prandtl-Ishlinskii Models

2.1 Introduction

A large number of phenomenological models have been proposed to characterize the hysteresis properties of smart actuators and ferromagnetic materials. The most cited phenomenological models include: the Preisach, Krasnosel'skii-Pokrovskii and Prandtl-Ishlinskii models. Unlike the Prandtl-Ishlinskii and Krasnosel'skii-Pokrovskii models, the Prandtl-Ishlinskii model exhibits continuous character, and thus offers a unique advantage in deriving the model inverse analytically that may be applied for hysteresis compensation [12]. Although the classic is limited to symmetric and unbounded hysteresis properties, alternate terms of the Prandtl-Ishlinskii have recently proposed for predict of asymmetric and bounded hysteresis [39]. The Prandtl-Ishlinskii model offers a unique property that could be vital for realizing real-time compensation of the hysteresis. This property is associated with the complementary nature of play and stop operators, which could be utilized to achieve hysteresis compensation in more sufficient manner through composition of the POPI and SOPI models. The Prandtl-Ishlinskii model can be constructed using either the play or stop hysteresis operators, although the reported hysteresis models of smart actuators are invariably based on the play operator, which exhibit counter-clockwise hysteresis loops symmetric about the input [12,39]. The Prandtl-Ishlinskii model based on the stop operator has also been reported to characterize hysteresis of materials which exhibit clockwise hysteresis loops [17]. This complementary property of the play and stop operators of the Prandtl-Ishlinskii model is

thus explored to seek compensation of nonlinearity hysteresis effects of smart actuator. In this chapter, the properties of play and stop operators are discussed and the corresponding Prandtl-Ishlinskii models are formulated. The concept of shape function is further implemented to derive the models.

2.2 Play operator based Prandtl-Ishlinskii (POPI) model

Similar to the Preisach model, as described in section 1.2, the Prandtl-Ishlinskii model is constructed using either play or stop operators. Unlike the discontinuous relay operator in the Preisach model, the play and stop operator are continuous hysteresis operators which are characterized by the input v and the thresholds r and s , respectively [17]. The classical Prandtl-Ishlinskii model can be formulated upon integration of either the play or stop operators. The models derived on the basis of the play and stop operators, however, exhibit different hysteresis properties which are introduced below for both play and stop operators. This is attributed to the properties of the play and stop hysteresis operators, which are presented in the following subsections.

2.2.1 PLAY OPERATOR

The play hysteresis operator is a continuous, rate independent and symmetric operator. This operator has been thoroughly described in [17]. Figure 2.2 illustrates the input-output characteristics of the play operator, as a function of the threshold r which is a positive constant. The threshold r determines the shape and the nature of the hysteresis nonlinearity. The input-output characteristics of the hysteresis operator have been related to different physical phenomena such as backlash in gear mechanisms. Consider a pair of gears with certain clearance (r_0-a) between the meshing teeth with motion of the driving

gear, v is the input (driving gear) to the driver gear which its output is z (Figure 2.1). The output corresponding to backward motion of the driving gear (towards to left in Figure 2.1) is mapped by the path $C-D$ in the output-input curve shown in Figure 2.2, provided in the driving gear motion is limited to (r_0-a) . As the input motion v exceeds the clearance (r_0-a) , both gears move together and map the path $D-A$. The output maps the path $A-B$ as the driving gear reverse its direction and its motion is limited to (r_0-a) . the output is mapped by the path $B-C$ as the input motion exceeds the clearance. The resulting output-input Figure 2.2 are described by the play operator with threshold r , representing the clearance (r_0-a) .

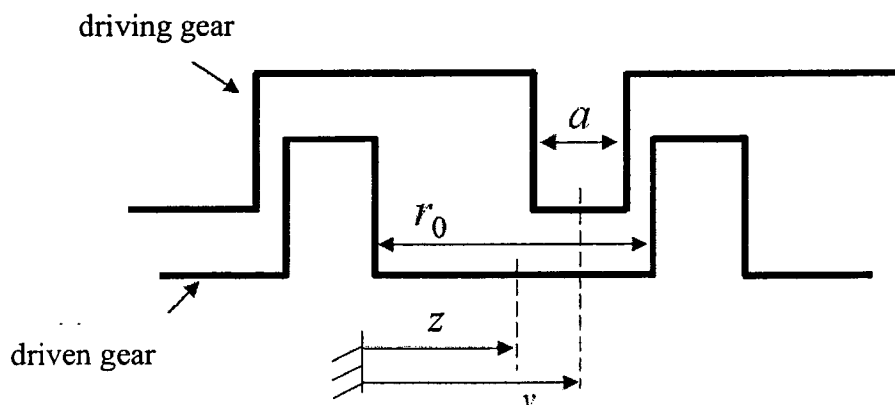


Figure 2.1: A gear mechanism illustrating the play operator behavior.

From Figure 2.2, it is evident the output is linearly related to input during the segments $B-C$ and $D-A$. The play operator describes the input-output relationships by a unity slope, while the output along the paths $B-C$ and $D-A$ follows a given direction. On the other hand, the outputs during the paths $D-C$ and $A-B$ will remain constant, irrespective of the changes in the input, while the output may follow both the directions.

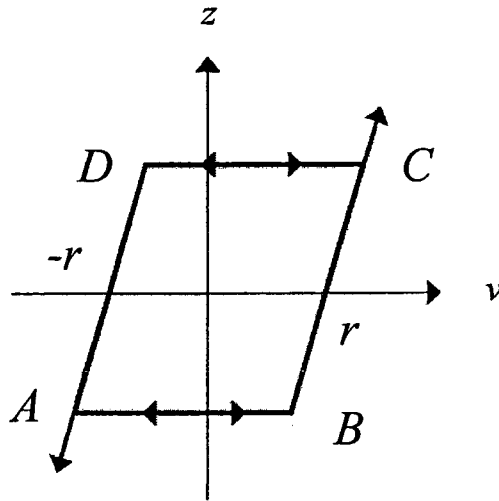


Figure 2.2: Input-output relationship of the play operator.

Analytically, for an input $v(t) \in C_m[0, T]$, where C_m represents the space of piecewise monotone continuous functions, such that the function v is a monotone in the sub-intervals $[t_i, t_{i+1}]$, the output of the play operator $z(t)$ is analytically expressed as [p.24,17]:

$$\begin{aligned}
 z(0) &= f_r(v(0)) \\
 z(t) &= f_r(v(t), z(t_i)); \quad 0 \leq i \leq N - 1 \\
 F_r[v](t) &= z(t)
 \end{aligned}
 \tag{2.1}$$

Where for $t_0=0 < t_1 < \dots < t_N = T$, and $F_r[v]$ is the operator; represents the number of sub-intervals in time; and $f_r(v): \mathfrak{R} \rightarrow \mathfrak{R}$ is defined as [p.25,17]:

$$f_r(v, z) = \max\{v - r, \min\{v + r, z\}\}
 \tag{2.2}$$

In the above definition, the argument of the operator F_r is written in square brackets to indicate the functional dependence, since it maps one function to another function. Some of the key properties of the play hysteresis operator are briefly described below:

- **Rate-independence:** The play operator $F_r[v]$ is a rate-independent hysteresis operator, such that [p.33,17] :

$$F_r[v] \circ B = F_r[v \circ B] \quad (2.3)$$

where B is a continuous increasing function, $B:[0, T]$, satisfying $B(0)=0$ and $B(T)=T$.

- **Lipschitz-continuity:** For a given input $v(t)$ and threshold $r \geq 0$, the output of the play operator (2.1) can be extended to Lipschitz continuous [p.47,17].
- **Memory effects:** The play operator is a hysteresis operator with nonlocal-memory effect, where the output of the operator depends on the current value of input as well as the past values of the output [17].

The output-input characteristics of the play operator are mathematically described by two continuous functions. The ascending path $B-C$ of the output-input curve in Figure 2.2 is expressed mathematically by $v(t)-r$, while the descending path $D-A$ can be expressed mathematically $v(t)+r$. The maximum and the minimum values of outputs of the play operator are directly dependent on the input v . Furthermore, the output z approaches zero in two cases, as observed in Figure 2.2 and Equation (2.1):

- $z=0$ for $v(t)=r$, in the ascending path $B-C$.
- $z=0$ for $v(t)=-r$, in the descending path $D-A$.

2.2.2 PLAY OPERATOR BASED PRANDTL-ISHLINSKII (POPI) MODEL

The Prandtl-Ishlinskii model utilizes the play operator $F_r[v](t)$ to describe a relationship between the output $\Phi[v](t)$ and input $v(t)$, such that:

$$n(t) = \Phi[v](t) = qv(t) + \int_0^R p(r)F_r[v](t)dr \quad (2.4)$$

where $n(t)$ is the output of the Prandtl-Ishlinskii model, $p(r)$ is a density function which satisfies $p(r) \geq 0$, and q is a positive constant $q > 0$. Both $p(r)$ and q are generally identified from the experimental data for a particular material or smart actuator.

The Prandtl-Ishlinskii model with the density function maps $C_m[t_o, \infty)$ into $C_m[t_o, \infty)$, and the density function $p(r)$ tends to vanish for greater values of r . The upper limit of integration is thus generally assumed as $R = \infty$ where the choice of $+\infty$ is just a matter of convenience [p.28,17]. Owing to the continuous property play operators, the POPI model can be implemented using only a few play hysteresis operators [12]. The output of the POPI model can be numerically derived from:

$$n(t) = \sum_{j=1}^{J_p} p(r_j)F_{r_j}[v](t) \quad (2.5)$$

where J_p is the number of the hysteresis operators considered, and $r_j (j=1, \dots, N)$ is the threshold values of the j^{th} operator.

Example 2.1: Properties of the play operator and the POPI model

Consider an input of the form $v(t) = 12\sin(4\pi t)$ over the interval $t \in [0, 8]$ to the Prandtl-Ishlinskii model that presented in Equations (2.4) and (2.5) the characteristics of the POPI model are obtained by consideration integration of only five play operators with threshold values $r_j = [1.6, 3.2, 4.8, 6.4, 8.0]$ a density function of the following form was chosen to obtain the model response:

$$p(r_j) = 2e^{-0.1r_j} \quad (2.6)$$

The simulations were performed assuming $q = 1.4$ and $\Delta t = 0.01$ s.

Figure 2.3(a) illustrates the outputs of the three of the operators ($r_j=1.6, 4.8, 8$), which variation in the density function with r is illustrated in Figure 2.3 (b). The results clearly show that the width of the output-input relation of the play operator is directly dependent upon r , and that $p(r)$ vanishes as r increases. Figure 2.3 (c) illustrates the output-input characteristics of the POPI model, desired from Equation (2.5), using J_p . The results show output-input major hysteresis loop attributed to the output of the play hysteresis operators, shown in Figure 2.3 (a). Furthermore, the hysteresis loops of the play operator-based Prandtl-Ishlinskii (POPI) model, presented in Figure 2.3 (c), exhibits a counterclockwise direction.

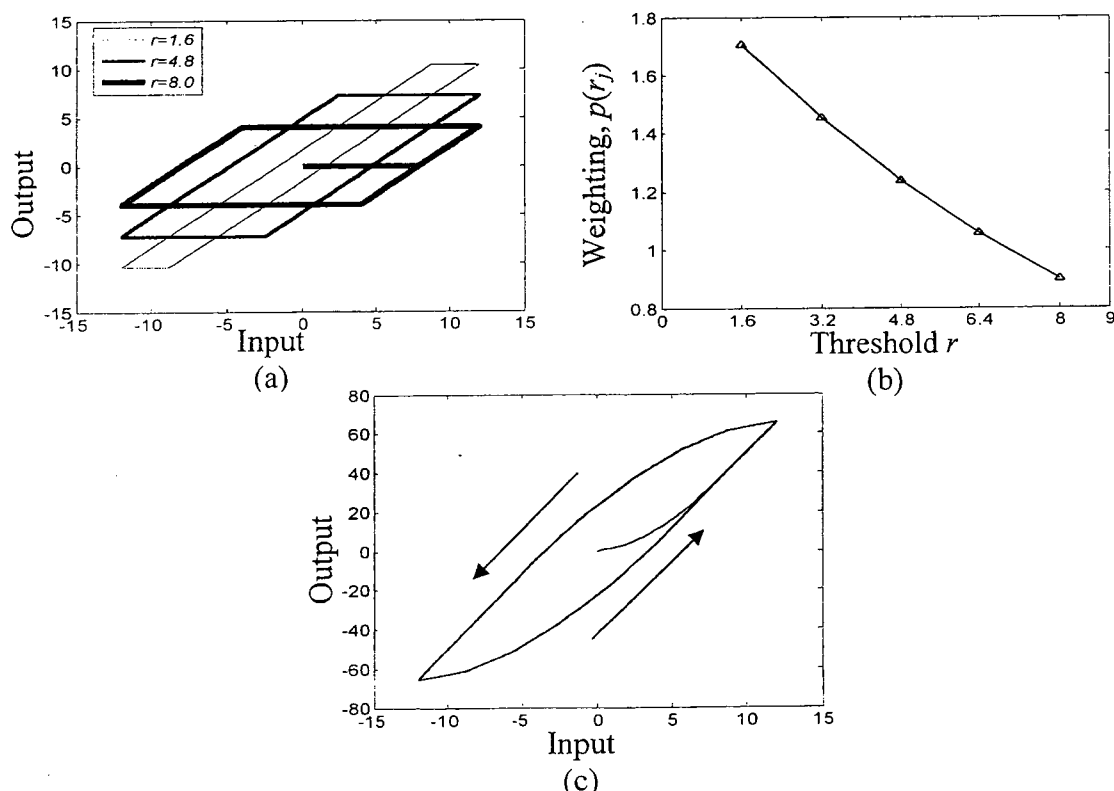


Figure 2.3: (a) Input-output relations of the play operators with different threshold values; (b) Variation in the density function with threshold r and ;(c) the output-input characteristics of the play operator based Prandtl-Ishlinskii (POPI) model under $v(t) = 12\sin(4\pi t)$.

2.3 Stop operator based Prandtl-Ishlinskii (SOPI) model

Although the hysteresis properties of smart materials actuators have been invariably characterized by the POPI model, the Prandtl-Ishlinskii hysteresis model may also be constructed using the stop operator. A few studies have considered the stop operator-based Prandtl-Ishlinskii model for describing hysteresis nonlinearity of materials [17]. Unlike POPI model, the output-input characteristics of the SOPI model exhibits clockwise hysteresis loops. This is attributable to the properties of the stop operator, which is discussed in the following subsections.

2.3.1 STOP OPERATOR

A stop operator proposed to characterize the elastic-plastic behavior in continuum mechanics [p.25,17]. The output-input relationship of a stop operator is illustrated in Figure 2.4, which could be interpreted by the elastic-plastic stress-strain relation of a material, from the figure, it may be deduced that the strain v is linearly related to stress w according to the Hook's law. Provided that the applied stress w is less than yield stress s of the material. The strain tends to remain constant as the stress w approaches or exceeds the yield stress. In the stop operator, the yield stress s is referred to output-input relations of a stop operator as the threshold similar to the play operator.

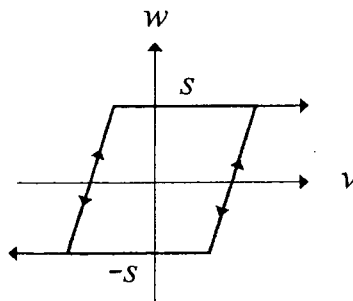


Figure 2.4: Stop operator.

Analytically, for an input $v(t) \in C_m[0, T]$, where C_m represents the space of piecewise monotone continuous function, such that the function v is monotone over the sub-intervals $[t_i, t_{i+1}]$, the output of the stop hysteresis stop operator $w(t)$ can be analytically expressed as [p26, 17]:

$$\begin{aligned} w(0) &= e_s(v(0)) \\ w(t) &= e_s(v(t) - v(t_i) + w(t_i)); \quad 0 \leq i \leq N-1 \\ E_s[v](t) &= w(t) \end{aligned} \tag{2.7}$$

Where $t_0=0 < t_1 < \dots < t_N = T$, $E_s[v]$ is operator, and:

$$e_s(v) = \min\{\max\{s, v\}, s\} \tag{2.8}$$

where $-s$ and s are the negative and the positive values of the threshold of the stop operator, respectively.

Some key properties of the stop hysteresis operator are briefly described below:

- **Rate-independence:** The stop operator $E_s[v]$ is a rate-independent hysteresis operator, such that [p.33,17] :

$$E_s[v] \circ B = E_s[v \circ B] \tag{2.9}$$

where B is a continuous increasing function, $B:[0, T]$, satisfying $B(0)=0$ and $B(T)=T$.

- **Lipschitz-continuity:** For a given input $v(t)$ and threshold $s \geq 0$, the output of the stop operator (2.8) can be extended to Lipschitz continuous [p.47, 17].
- **Memory effects:** The stop operator is a hysteresis operator with nonlocal-memory effect, where the output of the operator depends not only on the current value of input but also on the past values of the output [17].

2.3.2 STOP OPERATOR-BASED PRANDTL-ISHLINSKII (SOPI) MODEL

The stop operator-based Prandtl-Ishlinskii (SOPI) model is formulated upon integration of stop operators $E_s[v]$ to describe a relationship between the output $\Gamma[v](t)$ and the input $v(t)$, such that :

$$m(t) = \Gamma[v](t) = \int_0^s g(s)E_s[v](t)ds \quad (2.10)$$

where $m(t)$ is the output of the SOPI model and $g(s)$ is the density function, which is positive and integrable. Owing to the continuous property of the stop operator, the SOPI model can be implemented using only a few stop hysteresis operators as in the case of the POPI model [12]. The output of the SOPI model can be numerically obtained from:

$$m(t) = \sum_{j=1}^{J_s} g(s_j)E_{s_j}[v](t) \quad (2.11)$$

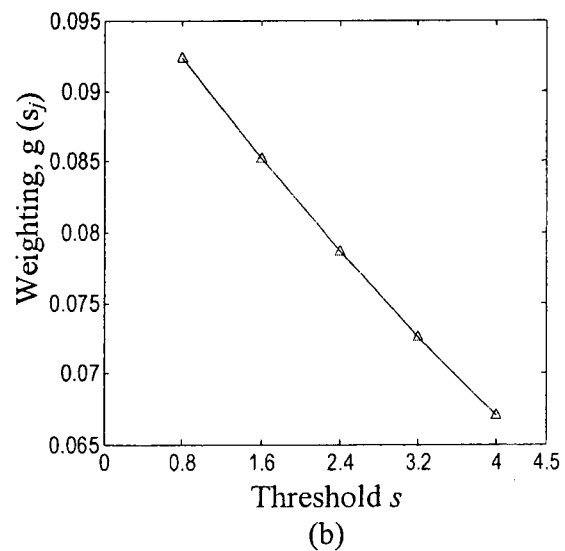
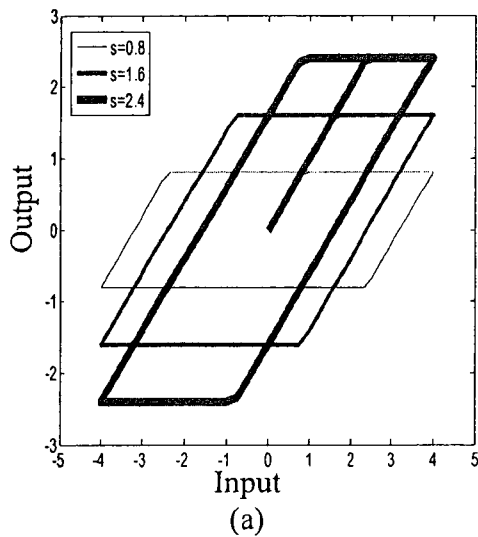
where J_s is the number of the hysteresis stop operators considered. The key properties of the stop operator and the stop operator based model are demonstrated through the following simulation example.

Example 2.2: Properties of the stop operator and the SOPI model

Consider an input of the form $v(t)=4\sin(4\pi t)$ over the interval $t \in [0,5]$ to the Prandtl-Ishlinskii model presented in Equation (2.11). The characteristics of the SOPI model are obtained by integration of only five stop operators with threshold values $s_j = [0.8, 1.6, 2.4, 3.2, 4.0]$. A density function of the following form was chosen to obtain the model response:

$$g(s_j)=0.1e^{-0.1s_j} \quad (2.12)$$

The simulations were performed assuming $\Delta t=0.01$ s. Figure 2.5(a) illustrates the outputs of the three of the operators ($s_j=0.8, 1.6, 2.4$), while the variation in the density function with s is illustrated in Figure 2.5 (b). The results clearly show that the width of the output-input relation of the stop operator is directly dependent upon s ; and that $g(s)$ vanishes as s increases. Figure 2.5 (c) illustrates the output-input characteristics of the SOPI model, derived from Equation (2.11), using $J_s=5$. The results show output-input major hysteresis loop attributed to the output of the stop hysteresis operators, shown in Figure 2.5 (a). Furthermore, the hysteresis loop of the stop operator-based Prandtl-Ishlinskii (SOPI) model, presented in Figure 2.5 (c), exhibits a clockwise direction.



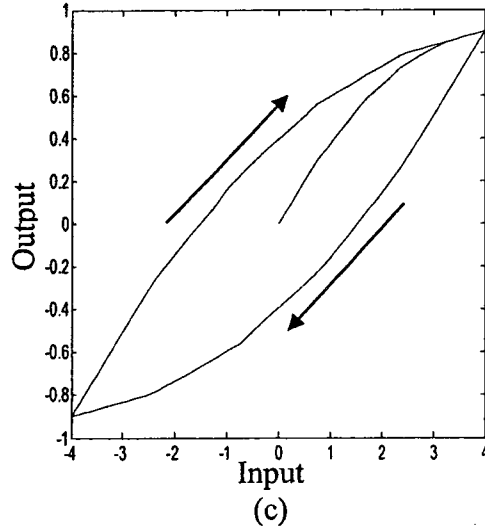


Figure 2.5: (a) Input-output relations of the stop operator with different threshold values; (b) variation in the density function with the threshold s ; and (c) Input-output characteristics of the stop operator based Prandtl-Ishlinskii (SOPI) model based under $v(t) = 4\sin(2\pi t)$.

2.4 Relationship between the play and stop operators

In general the play and the stop operators are characterized by input v , the thresholds r and s respectively. A relationship between the play and stop operators could be formulated using the definitions of the operators, given by:

$$f_r(v) = \max\{v - r, \min\{v + r, z\}\} \quad (2.13)$$

$$e_s(v) = \min\{\max\{-s, v\}, s\} \quad (2.14)$$

Considering identical values of the thresholds $s = r$, the two operators may be related, such that [p.26, 17]:

$$\begin{aligned} v - f_r(v, z) &= v - \max\{v - r, \min\{v + r, z\}\} \\ &= \min\{r, \max\{-r, v - z\}\} \\ &= e_r(v - z), \end{aligned} \quad (2.15)$$

for any piecewise monotone input v , it can it has been shown that :

$$F_r[v](0) + E_r[v](0) = f_r(v(0), 0) + e_r(v(0)) \quad : \text{ for } t \in [t_i, t_{i+1}] \quad (2.16)$$

$$\begin{aligned} F_r[v](t) + E_r[v](t) &= f_r(v(t), F_r[v](t_i)) + e_r(v(t) - v(t_i) + E_r[v](t_i)) \\ &= f_r(v(t), F_r[v](t_i)) + e_r(v(t) - F_r[v](t_i)) \\ &= v(t) \end{aligned} \quad (2.17)$$

Equation (2.17) is referred to the complementary property of the stop and play operators. Appendix A summarized proof for the complementary property. The complementary property could be established only for the special case $s=r$. this relation, however, would not be valid for the general case, $s \neq r$.

2.5 Model formulation using shape function

The complementary property of the stop and play operators, illustrated in Equation (2.17), cannot be directly applied for compensations of hysteresis effects, which would involve the composition of the SOPI and POPI models. Moreover, the stated complementary property is considered valid only when the play and stop operators have identical threshold values. Alternatively, the shape functions of the output-input characteristics of the play and stop operator-based models may be explored to achieve a unity value of their composition.

In this section, the shape function concept is thus introduced for alternative formulations of the POPI and SOPI models. The shape function is essential for identifying the shapes of the hysteresis loops. Shape functions of the hysteresis models generally indicate the direction of the input-output hysteresis curves, which can be shown

to be complementary for the SOPI and POPI models. The initial loading curves for the POPI and SOPI models are employed in order to illustrate follow employed in order to illustrate that the input-output curves of POPI and SOPI models follow counterclockwise and clockwise paths, respectively. The initial loading curve is defined when the initial state of the Prandtl-Ishlinskii model is zero and when the input increases monotonically. The shape function for the SOPI model has been defined using the shape function of the stop operator ψ_e and the density function $g(s)$, as [p.92, 17]:

$$\theta_e(x) = \int_0^{\infty} g(s)\psi_e(x)ds \quad (2.18)$$

where θ_e is the shape function of input variation x for the Prandtl-Ishlinskii model based on the stop operator, and $\psi_e: \mathfrak{R} \rightarrow \mathfrak{R}$ is a continuous and odd function, expressed as [p.92, 17]:

$$\psi_e(x) = \int_s^{\infty} g(q)dq \quad (2.19)$$

substituting for ψ_e in (2.19) yields:

$$\theta_e(x) = \int_0^x \int_s^{\infty} g(q)dqds \quad (2.20)$$

Then second derivative of the shape function in (2.20) with respect to the input variation x , yields:

$$\theta_e''(x) = g(\infty) - g(x) \quad (2.21)$$

considering that the density function $g(\infty) \rightarrow 0$, the above reduces to the density function:

$$\theta_e''(x) = -g(x) \quad (2.22)$$

Owing to the positive density function, the above suggests that the shape function θ_e is a concave function. Furthermore, the shape function yields clockwise hysteresis loops. It can thus be concluded that the hysteresis loops given by the SOPI model would be concave clockwise loops.

In a similar manner, the shape function of the POPI model can be formulated using the shape function of the play operator ψ_f and the density function $p(r)$, as [17]:

$$\theta_f(x) = \int_0^{\infty} p(r)\psi_f(x)dr \quad (2.23)$$

where $\psi_f: \mathfrak{R} \rightarrow \mathfrak{R}$, is a continuous and odd function defined as [p.87, 17]:

$$\psi_f(x) = \text{sgn}(x) \max(|x| - r, 0) \quad (2.24)$$

The shape function of the POPI model has also been expressed as [p.88, 17]:

$$\theta_f(x) = p(0)x + \int_0^x p(r)(x-r)dr \quad (2.25)$$

The second derivative of the above shape function θ_f with respect to x reduces to the density function $p(r)$ as in the case of the SOPI model [p.88, 17]:

$$\theta_f''(x) = p(x) \quad (2.26)$$

Owing to the positive density function, the above suggests that the shape function $\theta_f(x)$ is a convex function. Upon substituting (2.26) in (2.25), the output of the POPI model can be derived in terms of the shape function θ_f as:

$$\Phi[v](t) = \theta_f'(0)v + \int_0^{\infty} \theta_f''(r)F_r[v](t)dr \quad (2.27)$$

Owing to the convex shape function, the hysteresis loops resulting from the POPI model (2.27) would be counter clockwise convex loops.

The concept of the initial loading curve and the properties of the shape function of the POPI and SOPI models are illustrated through follow simulation examples.

Example 2.3: Shape function of the POPI model

Consider the POPI model, presented in section 2.2.2, subject to a harmonic input, $v(t)=12\sin(4\pi t)$ over the interval $t \in [0,2]$. Further, consider a density function of the form $p(r_j) = 2e^{-0.1r_j}$, and integration of five play operators with threshold values, $r_j = 1.6, 3.2, 4.8, 6.4$ and 8 , and the outputs of the resulting POPI model are obtained through simulations using $\Delta t=0.0001$ s. The initial loading curve of this model is illustrated in Figure 2.6 the POPI model can be formulated using the shape function of the play operator ψ_f and the density function $p(r)$ as in eqn. (2.23).

Example 2.4: Shape function of the SOPI model

Consider the SOPI model, presented in section 2.3.2, subject to a harmonic input, $v(t)=4\sin(4\pi t)$ over the interval $t \in [0,2]$. Further, consider a density function of the form $g(s_j) = 2e^{-0.1s_j}$, and integration of five stop operators with threshold values, $s_j = 0.8, 1.6, 2.4, 3.2$ and 4.0 , and the outputs of the resulting SOPI model are obtained through

simulations using $\Delta t=0.0001$ s. The initial loading curve of this model is illustrated in Figure 2.7.

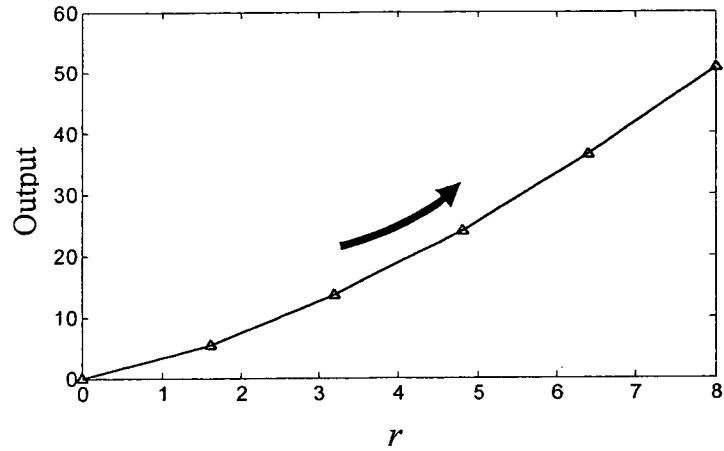


Figure 2.6: Input-output characteristics of initial loading curve ψ_f (2.25).

Figure 2.6 illustrates that the shape function of the POPI model is convex, Owing to the convex shape function the hysteresis loops resulting from the POPI model would be counter clockwise loops when the model integrates the play operator at different threshold values, while Figure 2.7 illustrates that the shape function of SOPI model is concave,

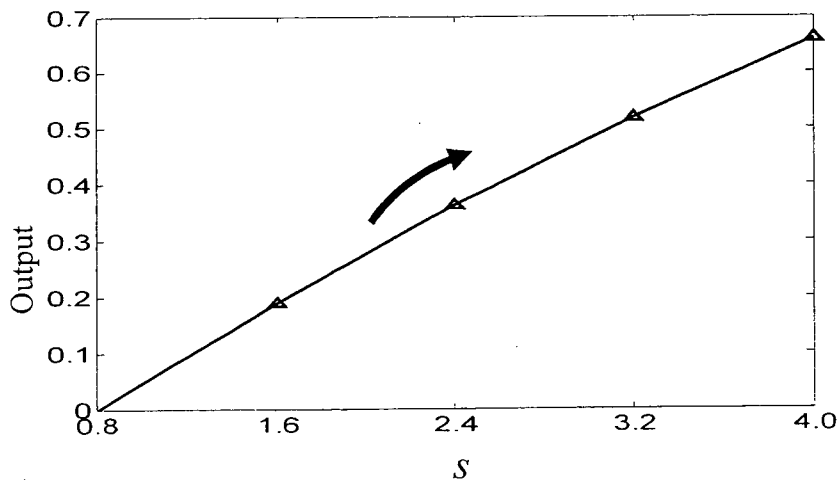


Figure 2.7: Input-output characteristics of initial loading curve ψ_e (2.19).

Owing to the concave shape function the hysteresis loops resulting from the SOPI model would be clockwise loops when the model integrates the stop operator at different threshold values. This result demonstrates that a composition between the SOPI and POPI models yields identity in input-output curves, this property will be utilized to compensate for hysteresis nonlinearities in POPI model.

2.6 Summary

The continuous play and stop hysteresis operators are defined and integrated to formulate Prandtl-Ishlinskii models. The properties of the operators and the models are illustrated through simple simulation examples, and the complementary property of the models based on stop and play operators is discussed for their identical threshold values. The concept of the shape function is further utilized to illustrate the shapes and directions of the initial loading curves of the stop- and play- operator based models. It is shown that the Prandtl-Ishlinskii based on play operator produces hysteresis loops with counterclockwise direction, while Prandtl-Ishlinskii model based on the stop operator yields loops with clockwise direction. Furthermore, the initial loading curves of the play and stop operator based models exhibit convex and concave shapes, respectively. Since the play operator based Prandtl-Ishlinskii model shows a counter clockwise direction in the input-output curves it will be implemented in chapter 3 to characterize the hysteresis nonlinearities of a piezoceramic actuator. The stop operator based Prandtl-Ishlinskii model with clockwise hysteresis loops will be investigated in chapter 4 to reduce the hysteresis effects in the piezoceramic actuator.

Chapter 3

Hysteresis Modeling of a Piezoceramic Actuator

3.1 Introduction

Piezoceramic actuators are increasingly being used in various applications micromachining [5,38,49,50], positioning in hard-disk drives and optical-memory devices [5,20,51], alignment of optical fibers [42,43,52,50,53] testing of microelectronic components and nanoscale metrology [44,14,54,58], micromachines [45,46,55], shape control in antennas [33], and biomedical testing [56]. Piezoceramic actuators offer nanometer resolution, high stiffness, and fast response when subject to a varying electrical field.

The Piezoceramic actuators, however, exhibit hysteresis nonlinearities between the applied input voltage and the output displacement. These effects could cause inaccuracies and oscillations in the system response, and could lead to instability of the closed loop system [3,19,44,53,57]. Considerable efforts have been made to characterize the hysteresis properties of the piezoceramic actuators in order to seek methods for enhancement of micropositioning precision and tracking performance. These have been resulted in a number of phenomenological models for describing the hysteresis nonlinearities of piezoceramic actuators. The Preisach model has been the most widely used model for describing the output-input hysteresis of piezoceramic actuators [2,3,20]. For instance, Hughes and Wen [2] proposed a Preisach model comprising a second-order density function to model the hysteresis nonlinearities of piezoceramic and SMA

actuators. Ge and Jouaneh [3] characterized the hysteresis in a piezoceramic actuator using modified relay operators with threshold values of 0 and +1 in the Preisach model. Alternatively, Galinaitis [16] used the Krasnosel'skii-Pokrovskii operator instead of the relay operator in the Preisach model to characterize and to compensate the hysteresis effects of a piezoceramic actuator. A few studies have employed Prandtl-Ishlinskii model to characterize the hysteresis nonlinearities in a piezoceramic actuator [39,48]. These studies have generally shown that the phenomenological models can accurately describe the hysteresis properties of smart actuators, while the model parameters are identified using the measured properties of the particular actuator. Among the most widely used phenomenological models such as Preisach, Krasnosel'skii-Pokrovskii and Prandtl-Ishlinskii, the Prandtl-Ishlinskii model offers a unique advantage that is beneficial for hysteresis compensation. Unlike the other models, the Prandtl-Ishlinskii model is analytically invertible. Its analytical inverse may thus be conveniently applied to seek hysteresis compensation. In this chapter, the measurements of the output-input characteristics of a piezoceramic actuator in the laboratory are described, and the measured data are presented to illustrate the hysteresis nonlinearities of the actuator. The parameters of the play operator-based Prandtl-Ishlinskii model are identified using the measured data and the model validity is demonstrated under harmonic input voltage.

3.2 Experimental characterization of hysteresis of a piezoceramic actuator

A piezoceramic actuator, P-753.31C manufactured by Physik Instrumente Company was considered for measurements of the hysteresis properties. The actuator provided maximum displacement of 100 μm from its static equilibrium position. The

actuator integrated a capacitive sensor for measurements of the actuator displacement response with sensitivity of $1\mu\text{m}/\text{V}$. The natural frequency of the piezoceramic actuator was specified by the manufacturer as 2.9 KHz. The excitation module voltage to the actuator was applied through a voltage amplifier (LVPZT, E-505), with a fixed gain of 10. The excitation voltage to the actuator ranged from 0 to 100 V.

The measurements of the actuator displacement response were performed in the laboratory under three different excitations. These included: (i) a harmonic excitation at a low frequency of 1 Hz, $v(t)=40\sin(2\pi t)$; (ii) a harmonic excitation at a higher frequency of 5 Hz, $v(t)=40\sin(10\pi t)$; and a complex harmonic excitation, $v(t)=5\sin(\pi t)+35\sin(2\pi t)$. The first two excitations were selected to identify the major loop output-input property of the actuator at two different frequencies, while the complex harmonic excitation was chosen to measure the major as well as minor hysteresis loops. Each excitation signal was synthesized in the ControlDesk platform and applied to the input amplifier. The actuator displacement response signal was acquired in the dSpace ControlDesk together with the input signal. Figure 3.1 illustrates the schematic of the measurement setup. The measured signals were subsequently analyzed to characterize the hysteresis properties of the actuator.

3.2.1 EXPERIMENTAL RESULTS

The time histories of the measured displacement responses in μm of the actuator under the selected three excitations are illustrated in Figure 3.2. The figure also shows the time histories of the applied voltage input in V. The results show very good agreements between the applied voltage and the measured displacement, which is attributed to unity sensitivity of the actuator and the displacement transducer ($1\mu\text{m}/\text{V}$).

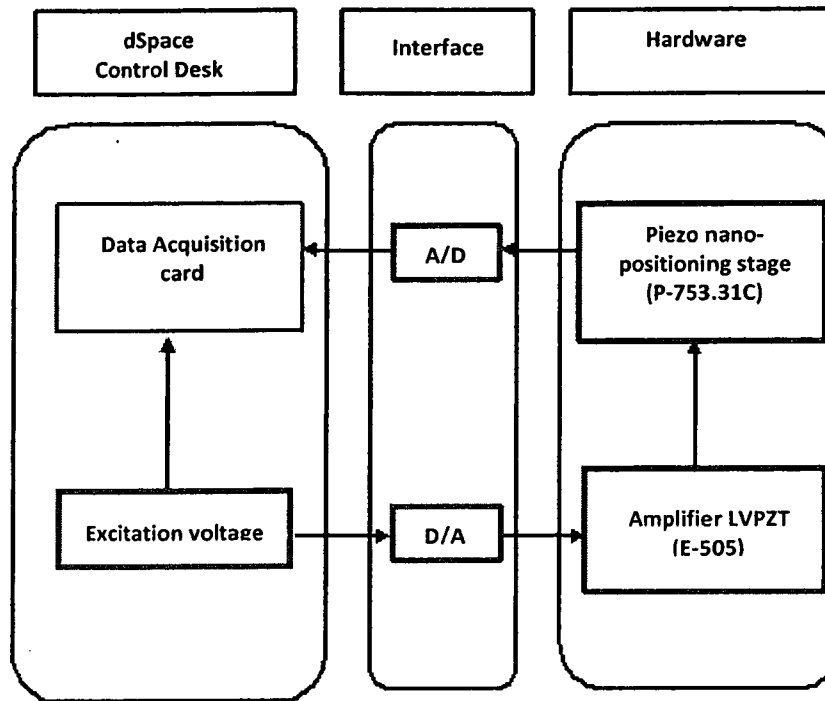


Figure 3.1: A schematic representation of the experimental setup.

The results, however, clearly show the phase difference between the input and the output, which is attributable to the actuator hysteresis. This is evident from the output-input characteristics of the actuator, shown in Figure 3.3. Figure 3.3 (a) and 3.3 (b) illustrate the major hysteresis loops relating the displacement response to the harmonic input voltages at 1 and 5 Hz excitation frequencies, respectively. The major as well as minor hysteresis loops are evident in Figure 3.3 (c) corresponding to the complex harmonic excitation. The experimental results clearly show the presence of hysteresis nonlinearities between the input voltage and the resulting output displacement.

Figure 3.3(a) presents that the major loop hysteresis is quantified by the peak hysteresis H and normalized with respect to peak-to-peak output M , Figure 3.4 (a), 3.4 (b),

3.4(c) illustrate the time-histories of the percent error between the input voltage and the measured displacement responses, respectively, corresponding to the three inputs;

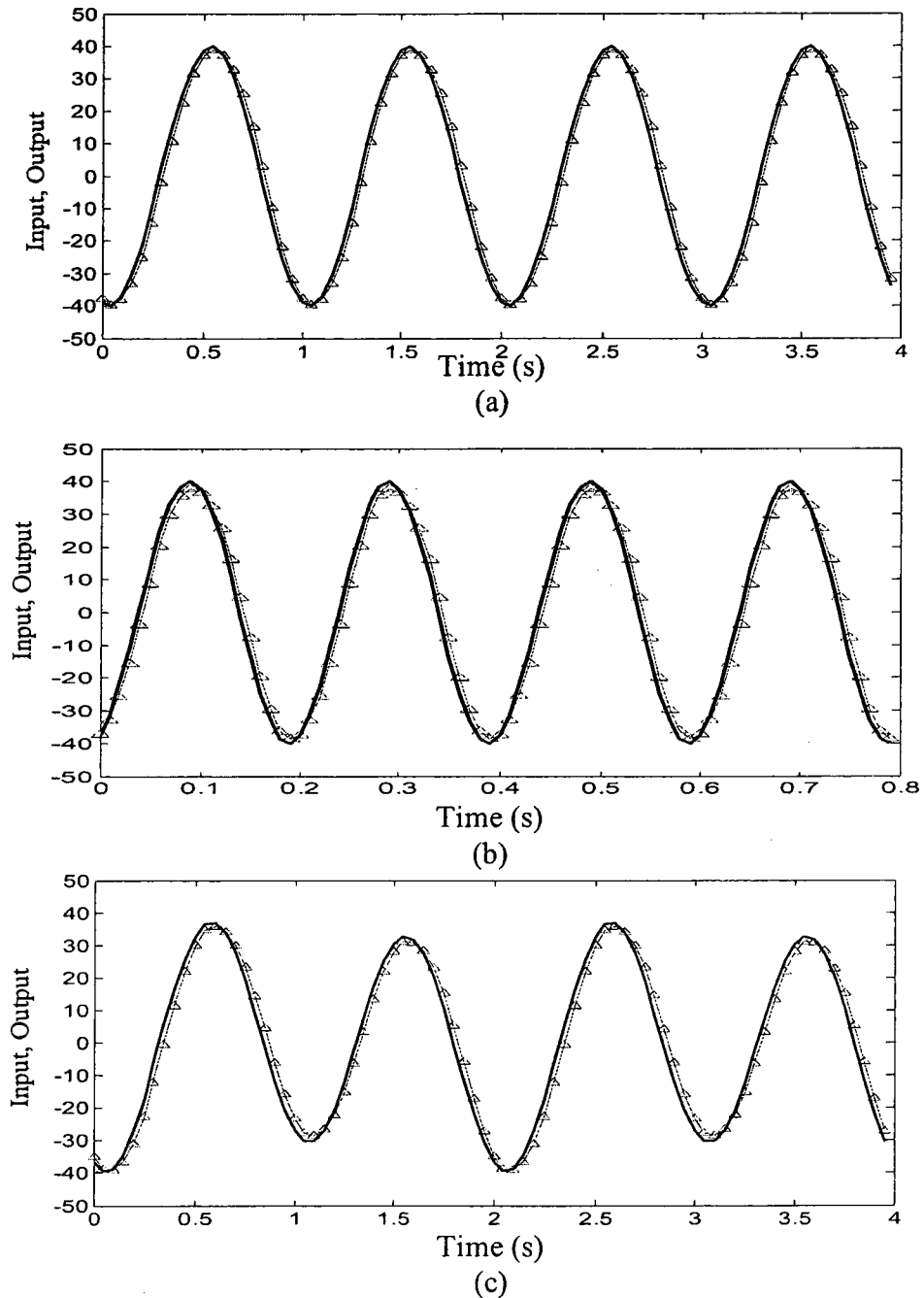


Figure 3.2: Time histories of the input voltage and output displacement responses of the piezoceramic actuator under different harmonic inputs (\triangle , output displacement; — , input voltage): (a) $v(t) = 40\sin(2\pi t)$; (b) $v(t) = 40\sin(10\pi t)$; and (c) $v(t) = 5\sin(\pi t) + 35\sin(2\pi t)$.

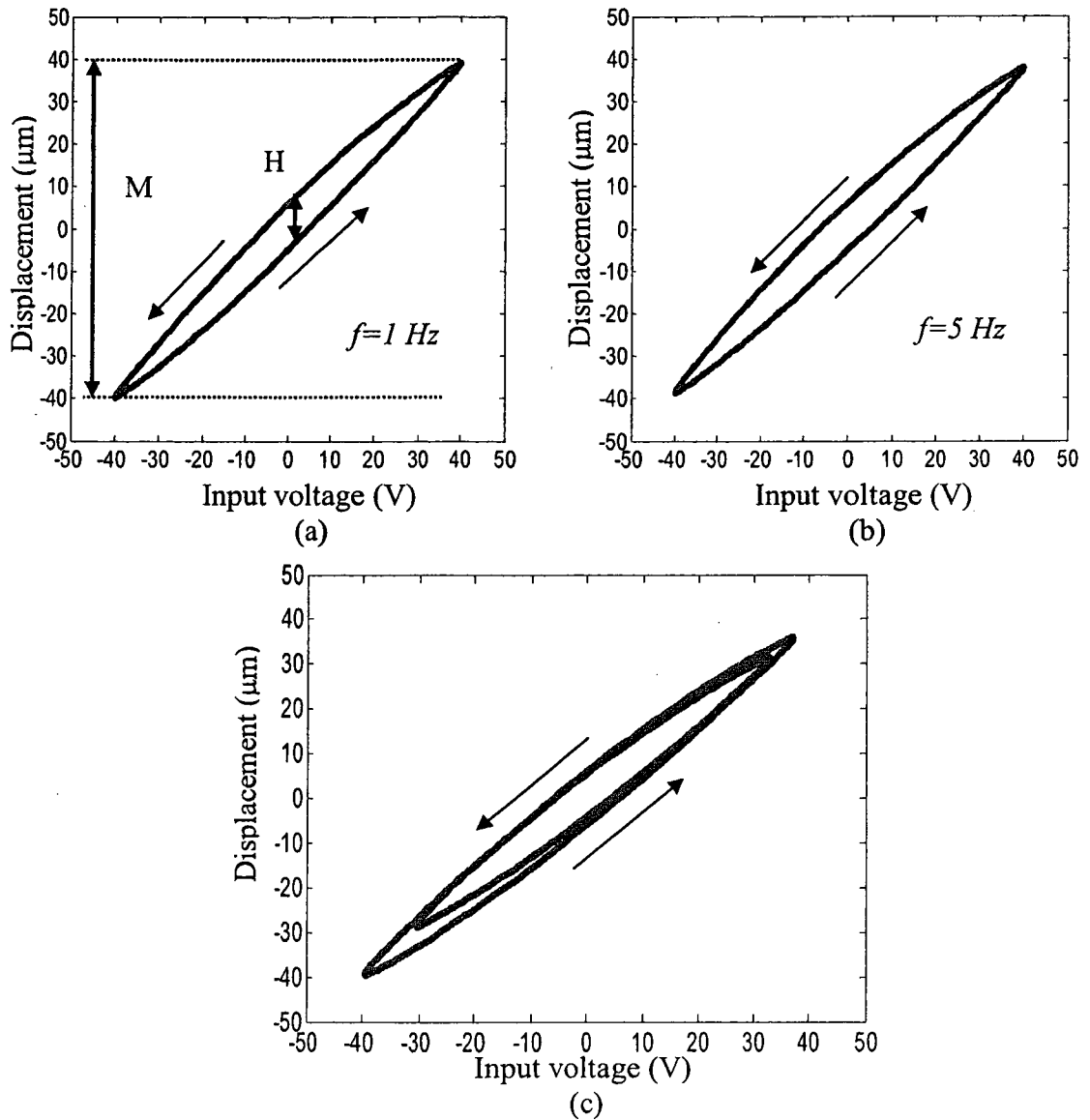
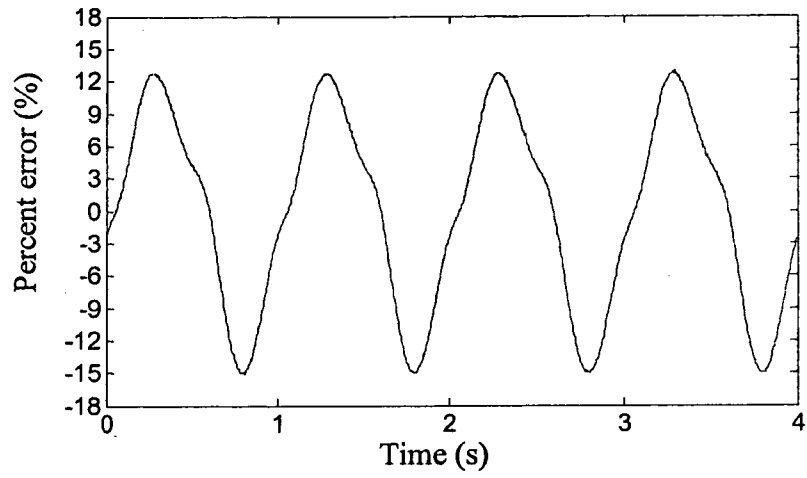
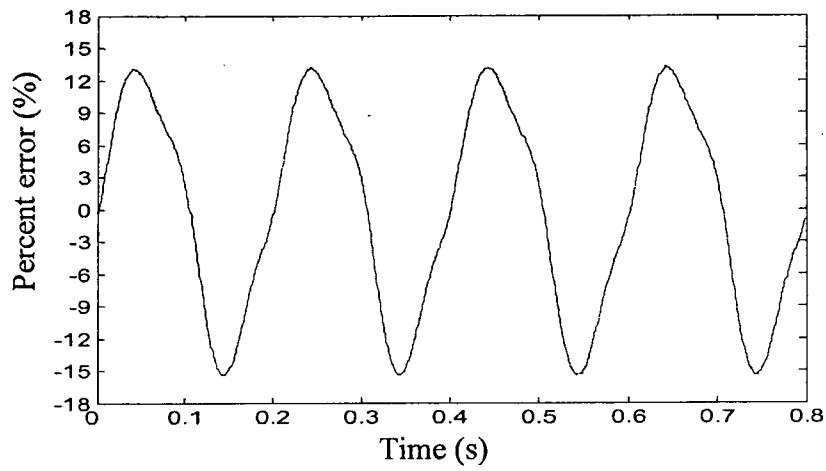


Figure 3.3: Measured input-output characteristics of the piezoceramic actuator under different sinusoidal inputs: (a) $v(t)=40\sin(2\pi t)$; (b) $v(t)=40\sin(10\pi t)$; and (c) $v(t)=5\sin(\pi t)+35\sin(2\pi t)$.

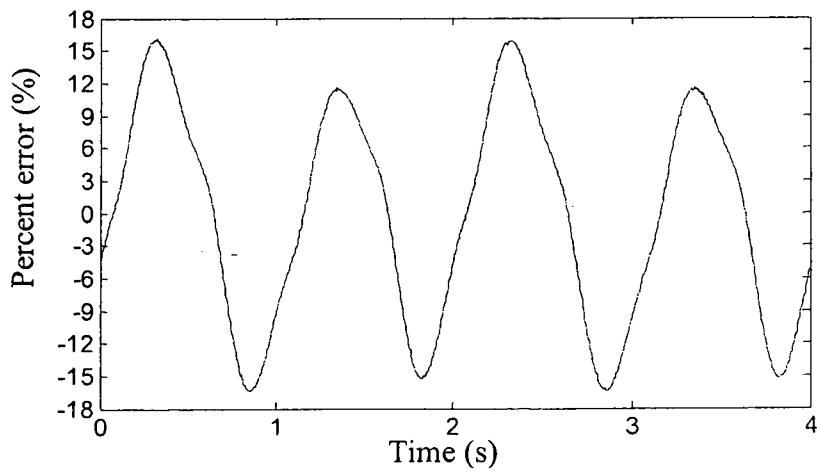
The results showed peak displacement percent errors of 14.65, 15.44 and 16.18 %, respectively, under the three inputs $v(t)=40\sin(2\pi t)$, $v(t)=40\sin(10\pi t)$, and $v(t)=5\sin(\pi t)+35\sin(2\pi t)$. Table 3.1 summarizes peak error magnitudes and peak percent error under the three inputs.



(a)



(b)



(c)

Figure 3.4: Time histories of percent errors in the output of the piezoceramic actuator due to the hysteresis nonlinearities under different inputs: (a) $v(t)=40\sin(2\pi t)$; (b) $v(t)=40\sin(10\pi t)$; and (c) $v(t)=5\sin(\pi t)+35\sin(2\pi t)$.

Table 3.1: The peak percent positioning error of the piezoceramic actuator.

Input signal $v(t)$	Peak percent positioning error (%)	Peak positioning error (μm)
$v(t)=40\sin(2\pi t)$	14.65	5.86
$v(t)=40\sin(10\pi t)$	15.44	6.17
$v(t)=5\sin(\pi t)+35\sin(2\pi t)$	16.18	6.47

3.2.2 MODELING HYSTERESIS NONLINEARITIES OF THE PIEZOCERAMIC ACTUATOR USING THE PRANDTL-ISHLINSKII MODEL

The hysteresis nonlinearity of the piezoceramic actuator could be accurately describing by the play operator based Prandtl-Ishlinskii model. The resulting model may be applied to seek a controller design for compensating the hysteresis-induced position error of the piezoceramic actuator. In this section, the Prandtl-Ishlinskii model based on the play operator (POPI), presented in section 2.2.2, is used to characterize the hysteresis of the piezoceramic actuator using the laboratory-measured output-input characteristics. The model is formulated using the density function of the following form:

$$p(r_j)=\alpha_j e^{-\beta_j r_j} \quad (3.1)$$

where α_j and β_j are positive constants. The threshold function of the play operator is chosen as a linearly increasing function, such that:

$$r_j = \sigma_r j; \quad j=1, 2, 3, \dots, J_p \quad (3.2)$$

where σ_r is a positive constant.

The parameters of the POPI model identified from the measured data. For this purpose, an error function of the position response of the model and the measured response is formulated and minimized. The error function is formulated as the error sum square, given by:

$$\Omega(X) = \sum_{i=1}^M [\Phi(v(i)) - Y_m(i)]^2 \quad (3.3)$$

where $\Phi(v(i))$ is the output of the Prandtl-Ishlinskii model under input $v(t) = 5\sin(\pi t) + 35\sin(2\pi t)$, $Y_m(i)$ is the measured displacement of the piezoceramic actuator and M is the number of data points considered. Ω is the error function for the major as well as minor hysteresis loops and X is the parameters vector given by: $\{X\} = \{a_1, \beta_1, q, \text{ and } \sigma_r\}$. The above error minimization problem was solved using MATLAB optimization toolbox, subjected to the following constrains:

$$q, a_1, \beta_1, \sigma_r > 0$$

The solution of the minimization problem were obtained for many different values of the starting vector and $J_p=10$. The resulting errors were examined to seek the minima. The solutions obtained for the different starting vectors, however, converged to very similar values of the model parameters, suggesting the global minimum. The resulting model parameters identified using the piezoceramic actuator data are presented in Table 3.2. The threshold values of operators and the corresponding density function are presented in Table 3.3. Figure 3.5 (a) shows the input-output characteristics of five of the play operators constructed under the input $v(t) = 40\sin(10\pi t)$, while Figure 3.5 (b) shows the variations in the density function values with the increasing threshold values. The results

show that the density function diminishes with increasing threshold value, while the width of the output-input of the play operator increases with r .

Table 3.2: Identified parameters of the Prandtl-Ishlinskii model based on the play operator.

Parameter	Value
σ_r	3.548
α_l	0.097
β_l	0.034
q	0.650

Table 3.3: Variations in the values of the thresholds and density function of the play operator based- Prandtl-Ishlinskii model.

Play operator number, j	Threshold, r_j	Density function value, $p(r_j)$
1	3.5475	0.0860
2	7.0950	0.0762
3	10.6425	0.0674
4	14.1900	0.0597
5	17.7375	0.0529
6	21.2850	0.0468
7	24.8325	0.0414
8	28.3800	0.0367
9	31.9275	0.0325
10	35.4750	0.0287

3.3 Model validation

The validity of the play operator based Prandtl-Ishlinskii model is investigated by comparing the model responses with the laboratory-measured data of the piezoceramic actuator under the chosen input voltages. Figure 3.6 illustrates comparisons of the Prandtl-Ishlinskii based play operator model with the measured data obtained under the three excitations considered in the laboratory measurements.

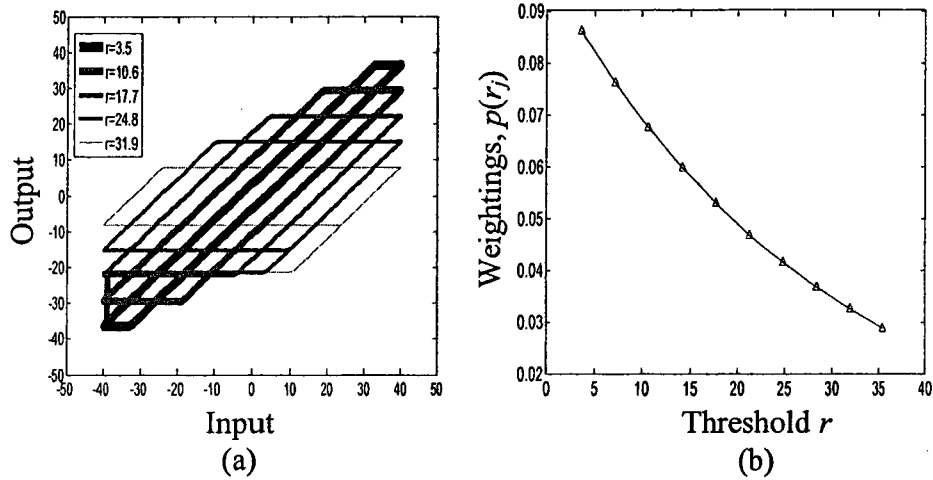


Figure 3.5: (a) Input-output characteristics of the play operators with different threshold values; and (b) Variations in the density function with the thresholds.

The results clearly suggest that the model can effectively predict the major as well as minor hysteresis loops properties of the piezoceramic actuator. Figure 3.6 (a) and 3.6 (b) illustrate a comparison of the major loops under $v(t)=40\sin(2\pi ft)$ at two different frequencies of 1 and 5 Hz. Figure 3.6 (c) illustrates comparison between the measured and model responses in major and minor hysteresis loops. The results suggest reasonably good agreements between the model and measured responses under the inputs considered, although slight errors between the responses are also evident.

The effectiveness of the Prandtl-Ishlinskii model in predicting the hysteresis responses of the piezoceramic actuator can also be seen from comparisons of the time-histories displacement responses of the model and the measured displacement, as shown in Figure 3.7 (a), 3.7(b) and 3.7(c). The figures present the comparisons of the model responses with the measured data for both simple and complex harmonic inputs considered in the simulation and laboratory measurements. The results show very good

agreements between the measured and model responses under all the three inputs. Slight errors, however, also occurred near the responses peaks. The errors between the measured data and the model displacement responses were computed in the domain and expressed as percent of the peak-to-peak displacement response corresponding to each input. Figure 3.8 (a), 3.8 (b), 3.8(c) illustrate the time-histories of the percent error between the model and measured displacement responses, respectively, corresponding to the three inputs; the results showed peak displacement errors of 1.44, 1.40, and 1.96 μm , respectively, under the three inputs $v(t)=40\sin(2\pi t)$, $v(t)=40\sin(10\pi t)$, and $v(t)=5\sin(\pi t)+35\sin(2\pi t)$. These correspond to peak errors of approximately 3.5% under the pure harmonic inputs and approximately 4.9% under the complex harmonic input. Table 3.4 summarizes peak error magnitudes, peak percent error and the percent norm error under the three inputs. From the results, it can be concluded that the Prandtl-Ishlinskii model based on the play operator can accurately design the hysteresis nonlinearities of the piezoceramic actuator.

Table 3.4: Summary of errors between the measured responses and the outputs of the play operator based Prandtl-Ishlinskii under the inputs considered.

Error type	harmonic input, $v(t)=40\sin(2\pi t)$	harmonic input, $v(t)=40\sin(10\pi t)$	Complex harmonic input, $v(t)=5\sin(\pi t)+35\sin(2\pi t)$
Maximum Error(μm)	1.44	1.40	1.96
Percent of maximum error (%)	3.60	3.51	4.90
Percent of Norm error (%)	2.35	2.86	3.43

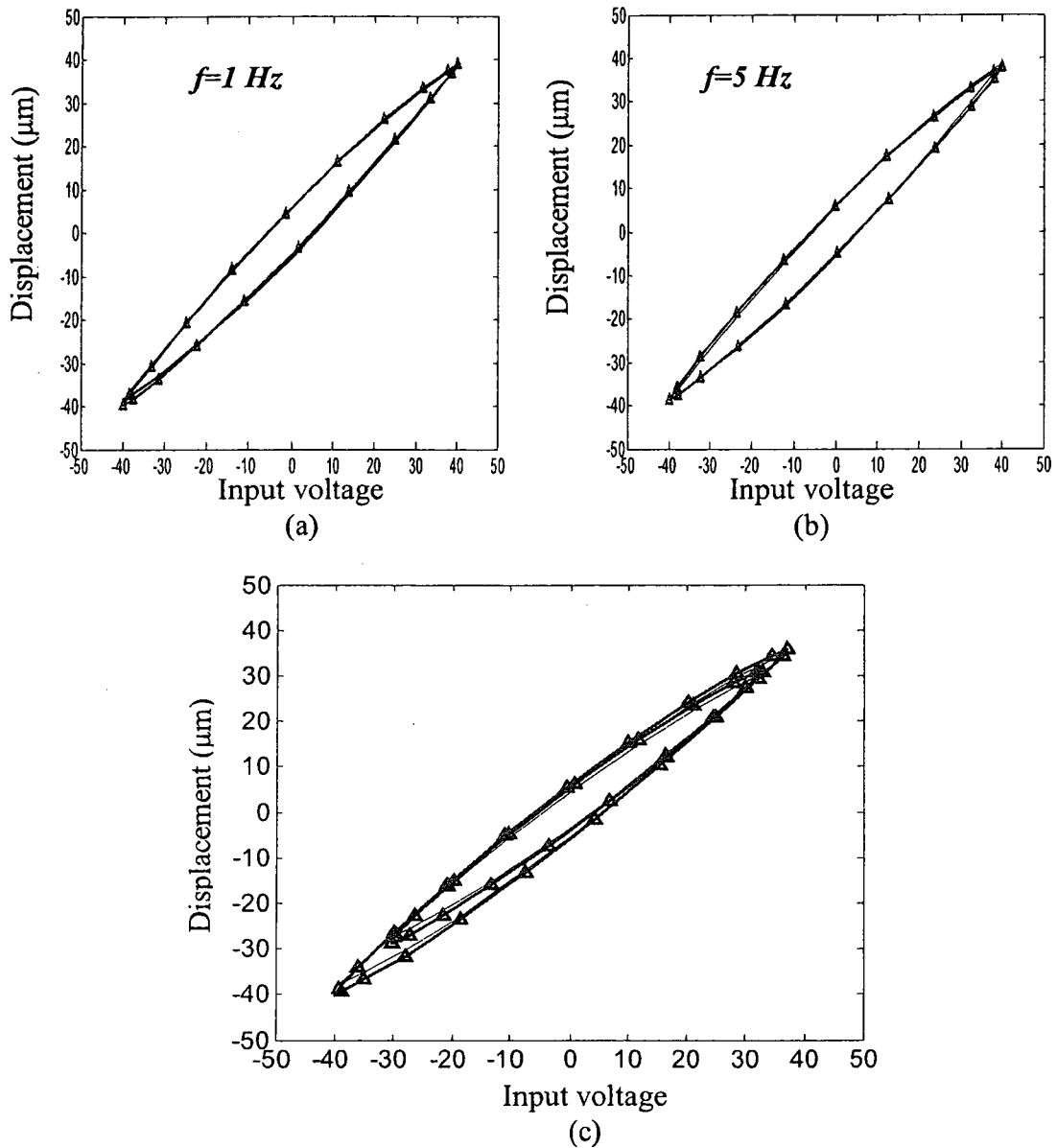
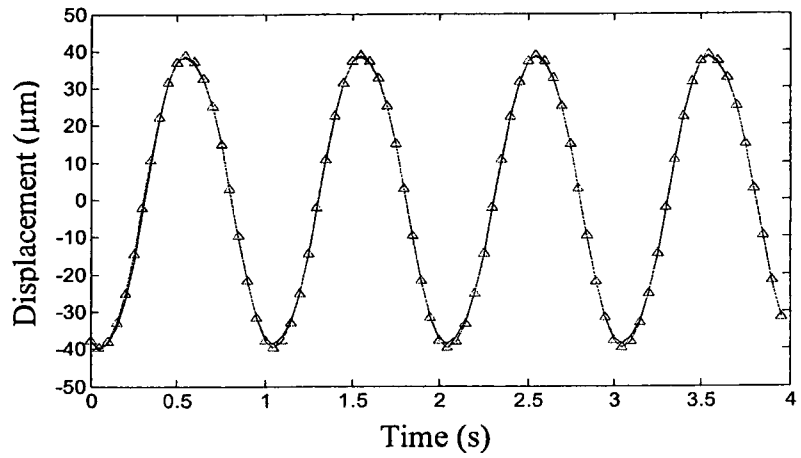
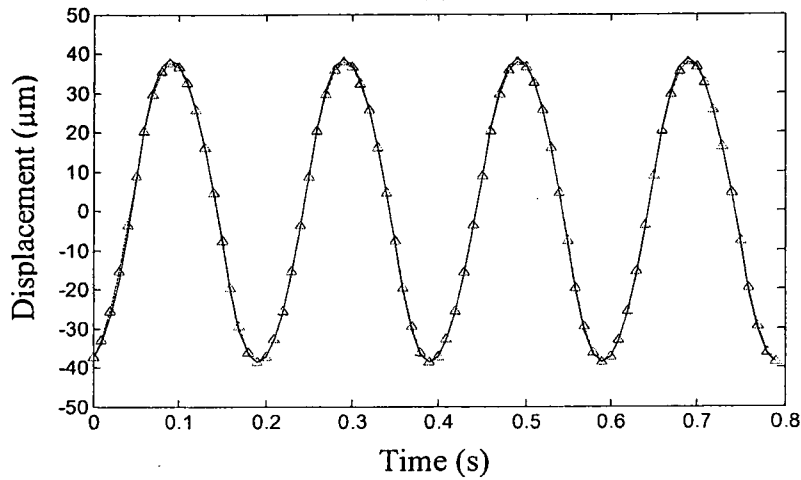


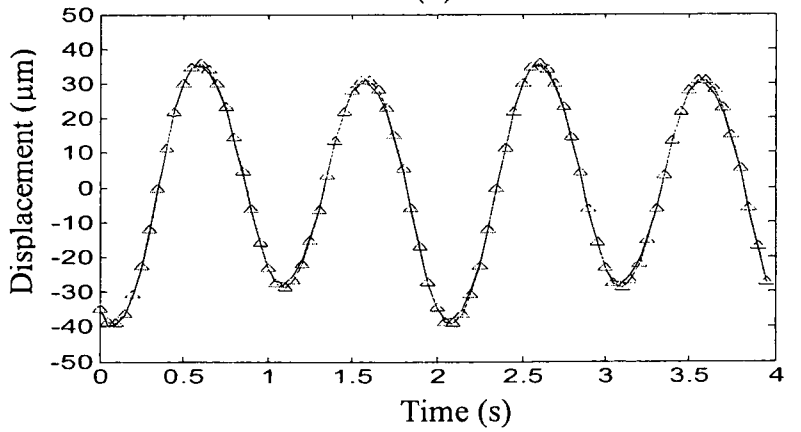
Figure 3.6: Comparisons between the measured displacement responses with the results derived from the Prandtl-Ishlinskii model under different sinusoidal inputs: (a) $v(t)=40\sin(2\pi t)$; (b) $v(t)=40\sin(10\pi t)$; and (c) $v(t)=5\sin(\pi t)+35\sin(2\pi t)$. (— \triangle —, measured; —, model).



(a)

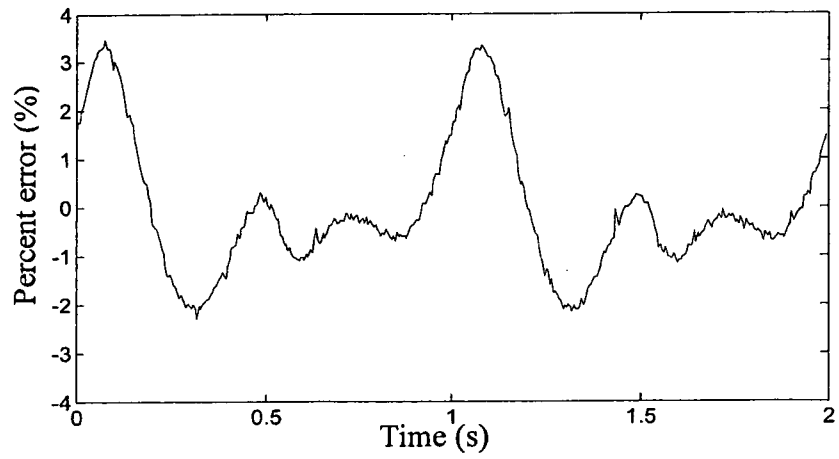


(b)

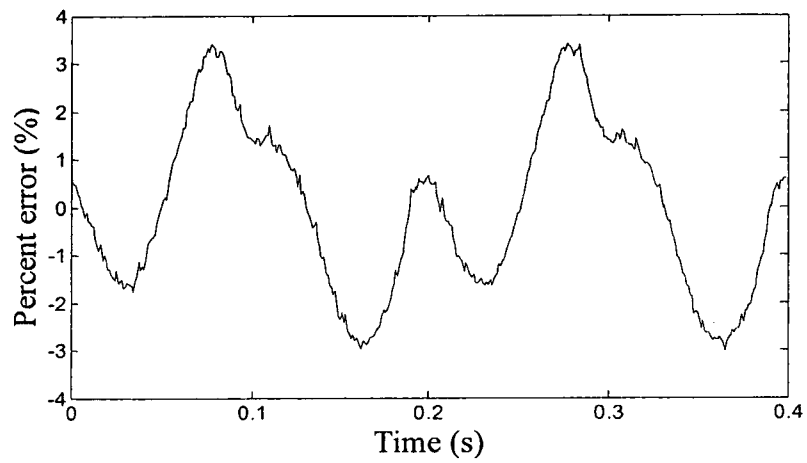


(c)

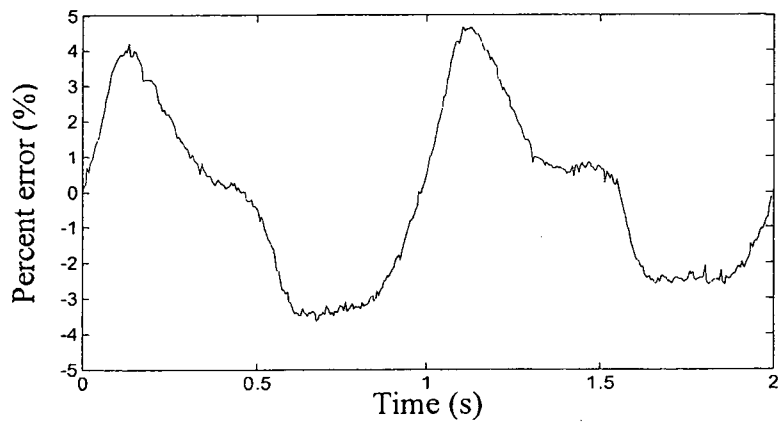
Figure 3.7 : Comparisons of time histories of measured displacement responses and the outputs of the play operator-based Prandtl-Ishlinskii model under different sinusoidal inputs: (a) $v(t)=40\sin(2\pi t)$ (b); $v(t)=40\sin(10\pi t)$; and (c) $v(t)=5\sin(\pi t)+35\sin(2\pi t)$ (— \triangle —, measured; —, model).



(a)



(b)



(c)

Figure 3.8 : Time-histories of percent displacement error under the three inputs: (a) $v(t)=40\sin(2\pi t)$; (b) $v(t)=40\sin(10\pi t)$; and (c) $v(t)=5\sin(\pi t)+35\sin(2\pi t)$.

3.4 Summary

Hysteresis properties of a piezoceramic actuator are characterized in the laboratory under harmonic inputs at two different frequencies. The measured data revealed strong hysteresis nonlinearities in the measured responses. The magnitude of hysteresis increased with excitation magnitude, while the effect of excitation frequency was observed to be small for the frequencies considered. The measured data was used to identify the parameters of the Prandtl-Ishlinskii model based on play operator through minimization of a sum squared function of error between the model and measured responses. The validity of the model structured using a total of 10 play operators was examined under different harmonic signals. Comparison of the model responses with the experimental data revealed very good agreements in both major as well as minor hysteresis loops under inputs at the selected frequencies. The peak prediction errors in the displacement response were in the order of 3.5% under harmonic excitations at 1 and 5 Hz, and nearly 4.9% under a complex harmonic input. The validated Prandtl-Ishlinskii model based on the play operator is used in conjunction with the stop operator based model in the following chapter to seek hysteresis compensation

Chapter 4

Compensation of Hysteresis Nonlinearities of a Piezoceramic Actuator

4.1 Introduction

The positioning accuracy of the piezoceramic actuators is limited due to the presence of hysteresis nonlinearities between the input voltage and the output displacement. The hysteresis nonlinearities of a piezoceramic actuator have been widely characterized and various control system design and synthesis have been proposed to reduce the effects hysteresis nonlinearities to enhance the tracking performance of the piezoceramic actuators [3,19,20,44]. The hysteresis compensation methods based on the inverse of the hysteresis model, applied as a feed-forward compensator in the open-loop and closed-loop control systems, have been widely proposed to compensate the effects of hysteresis nonlinearities of a piezoceramic actuator [2,7,20]. These studies have employed the inverse of the Preisach, Krasnosel'skii-Pokrovskii and Prandtl-Ishlinskii models to compensate for the hysteresis nonlinearities of the piezoceramic actuators. Ping and Ge [7] applied the inverse Preisach model as a feedforward compensator with a PID controller to reduce the hysteresis effects of a piezoceramic actuator. Galinaities [16] proposed the Krasnosel'skii-Pokrovskii operator instead of the relay operator in the Preisach model to characterize and to compensate the hysteresis effects of a piezoceramic actuator. Song et al. [62], in a similar manner, applied the inverse Preisach model in conjunction with a lag-lead controller for compensation of hysteresis effects in a piezoceramic actuator. The above studies have applied the numerical inversions of the

Preisach and Krasnosel'skii-Pokrovskii models to seek hysteresis compensation. The numerical inversions represent an approximation and may lead to certain error. Moreover, a numerical inverse is considered valid only in the vicinity of the conditions used in deriving the inverse. Alternatively, an exact inverse of the Prandtl-Ishlinskii may be derived analytically, although its application in hysteresis compensation has been explored in only a few studies [40]. Janocha and Kuhnen [35] compensate for the hysteresis effects of a piezoceramic actuator. The inverse Prandtl-Ishlinskii model, employed in the study, however, was constructed numerically. Krejci and Kuhnen [12] applied the Prandtl-Ishlinskii model to characterize and compensate hysteresis nonlinearities of a piezoceramic actuator. A few recent studies have applied the exact analytical inverse of the Prandtl-Ishlinskii model in compensating the hysteresis effects of a clan of smart actuators under varying sets of inputs [39,40].

In this chapter the compensation of the hysteresis nonlinearities is carried out by implementing the stop operator based Prandtl-Ishlinskii model as a feedforward compensator. This compensator is constructed using the parameters of play operator based Prandtl-Ishlinskii model presented in Chapter 3.

4.2 Compensation methodology

In this section, the stop operator based Prandtl-Ishlinskii model Γ is introduced as a feedforward compensator for the purpose of mitigating the hysteresis nonlinearities described by the play operator based Prandtl-Ishlinskii model Φ , presented in chapter 3. The hysteresis between the applied input and the output displacement in the piezoceramic actuator revealed counter clockwise loops in input-output curves. Similar counter

clockwise hysteresis loops have also been observed for a clan of smart actuators such as magnetostrictive actuators exhibiting current-to-displacement hysteresis loops [21], and the input temperature and the output displacement hysteresis loops of the SMA [14]. Such hysteresis effects may be offset by the SOPI model, where the output reveals loops in the clockwise direction, as illustrated in chapter 2. The hysteresis compensation effectiveness of the SOPI model is thus investigated by introducing it as a feedforward compensator preceding the actuator hysteresis described by the POPI model, as shown in Figure 4.1. The concept of a compensator for the hysteretic system is defined from: *a system Y is referred to as a compensator of a system X such that the series connection of Y and X would yield an identity transformation starting from initial states y_0 and x_0 , irrespectively, of Y and X.*

Given a desired input trajectory $v(t)$ and an initial condition $\Phi(0)$ for the play operator-based Prandtl-Ishlinskii model Φ , the stop operator-based Prandtl-Ishlinskii model Γ generates $z(t)$ as the input to the POPI model Φ . The objective is to obtain an identity mapping, i.e., $\Phi \circ \Gamma \approx I$, between the desired input $v(t)$ and the actual output $u(t)$, such that :

$$u(t) = \Phi \circ \Gamma [v](t) \quad (4.1)$$

where ‘ \circ ’ denotes the composition between both the models. In other words, the hysteresis nonlinearities of the play operator based Prandtl-Ishlinskii model with thresholds r_j and density function $p(r_j)$ can be compensated via the stop operator based Prandtl-Ishlinskii model with thresholds s_j and density function $g(s_j)$. For the desired input values $v_0, v_1, v_2, \dots, v_m$, and given thresholds $r_0, r_1, r_2, \dots, r_n$ and density function

values $p(r_0), p(r_1), p(r_2), \dots, p(r_n)$ of the play operator based Prandtl-Ishlinskii model, the stop operator based Prandtl-Ishlinskii model of thresholds $s_0, s_1, s_2, \dots, s_n$ and density function values $g(s_0), g(s_1), g(s_2), \dots, g(s_n)$ can be applied to compensate the hysteresis of the POPI model. The application of the SOPI model, however, requires the identification of its parameters, s_j and $g(s_j)$. Unlike the POPI model whose parameters could be identified from the measured hysteresis properties, the identification of SOPI model parameters could be more challenging. The suitability of the SOPI model compensator for reducing the hysteresis effects is initially explored using assumed model parameters. The simulation results are discussed in the following section to illustrate its potential applicability as a feedforward compensator.

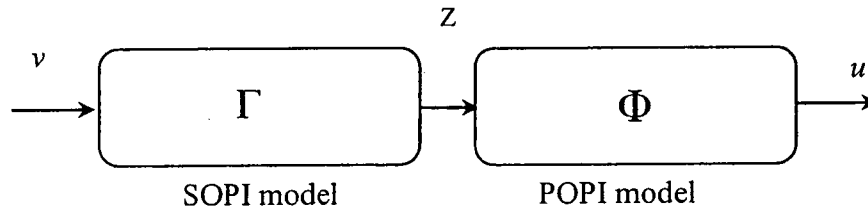


Figure 4.1: Illustration of hysteresis compensation via stop operator based Prandtl-Ishlinskii model.

4.3 Hysteresis Compensation Effectiveness of SOPI model

The following two subsections present the effectiveness of the SOPI model as a compensator for the hysteresis described by the POPI model. The first subsection utilizes the SOPI model using arbitrary parameters, while subsection 4.3.2 utilizes the SOPI model as a compensator on the basis of known POPI model parameters.

4.3.1 HYSTERESIS COMPENSATION USING SOPI MODEL WITH PARAMETERS IDENTICAL TO THAT OF THE POPI MODEL

Simulations are performed to evaluate the effectiveness of the SOPI model as a feedforward compensator for the hysteresis, which is characterized using the POPI model. A simulation example is considered to illustrate the feasibility of the SOPI model as a compensator. The example considers identical threshold and density functions of the SOPI and POPI models, such that:

$$r_j = s_j = \sigma_a j, \quad j = 0, 1, 2, \dots, J \quad (4.2)$$

$$p(r_j) = g(s_j) = \alpha_a e^{-\beta_a r_j} = \alpha_a e^{-\beta_a s_j} \quad (4.3)$$

where σ_a , α_a and β_a are arbitrary positive constants and $J = J_s = J_p$ is the number of the hysteresis operators considered in the model.

The simulation parameters for the numerical example were taken as: $\sigma_a = 0.5$; $\alpha_a = 0.1$; $\beta_a = 0.03$; $T = 2s$; and $\Delta t = 0.001$. Both models were formulated using a total of 20 operators ($J = 20$), while the solutions were attained under the input $v(t) = 10\sin(2\pi t)$. Figure 4.2 (a) and (b) illustrate the hysteresis loops between the input and the outputs of the SOPI and the POPI models, Γ and Φ , respectively. The input-output characteristics of the SOPI model exhibits clockwise hysteresis loop, as shown in Figure 4.2 (a) which is attributed to the property of the stop operator. The POPI model, on the other hand, exhibits counter clockwise hysteresis loops, as seen in Figure 4.2 (b), which is attributable to the property of the play operator. From the results, it is further seen that the initial loading curve of the POPI is convex, while that of the SOPI model is concave. Consequently, the POPI model may be used to characterize hysteresis nonlinearities, while the SOPI model could be applied to mitigate the hysteresis effects.

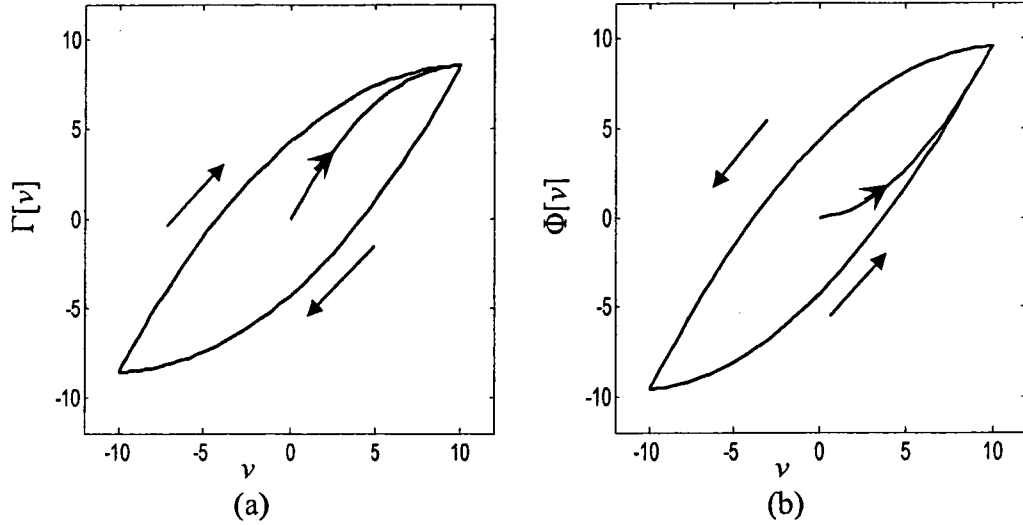


Figure 4.2: Input-output characteristics of: (a) the SOPI model; and (b) the POPI model under $v(t)=10\sin(2\pi t)$.

Subsequent simulations are performed by introducing the SOPI model as a feedforward compensator as shown in Figure 4.1. The output of the SOPI model $\Gamma[v](t)$, shown in Figure 4.2 (a), is applied as the input signal to the POPI model, i.e. $\Phi[\Gamma[v]](t)$. The resulting output of the compensation is shown in Figure 4.3 (c) together with the input-output responses of the SOPI and POPI models. The results suggest that application of the SOPI model helps reducing the hysteresis in the output significantly, although the SOPI model was based on arbitrary parameters. This is attributable to the opposing direction of the hysteresis loops of the SOPI model when compared to that of the POPI model.

4.3.2 HYSTERESIS COMPENSATION EFFECTIVENESS OF THE IDENTIFIED SOPI MODEL

The compensation ability of the SOPI model compensator could be considerably enhanced through identification of appropriate model parameters on the basis of the known POPI model. In this study, an error minimization problem is formulated and

solved to identify the parameters of the SOPI model that could serve as a feedforward compensator of the hysteresis effects.

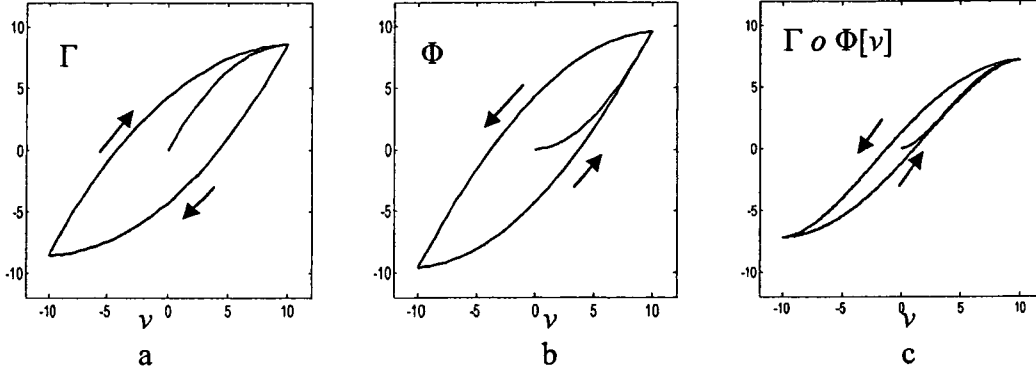


Figure 4.3: Compensation of hysteresis nonlinearities described by a POPI model output $\Phi[v](t)$ presented in Figure 4.2(b) using the SOPI model $\Gamma[v](t)$ presented in Figure 4.2(a).

A minimization function is formulated as the sum of squares of errors between the composition of the outputs of the POPI model Φ and the SOPI model Γ , and the input $v(i)$ such that:

$$\Lambda(Q) = \sum_{i=1}^M [\Phi \circ \Gamma_c[v](i) - v(i)]^2 \quad (4.4)$$

where Λ is the objective function of sum of squared errors to be minimized, Q is the parameters vector, M is the number of data points considered in the error minimization and Γ_c is the SOPI model which its parameters identified on the basis of known POPI model. The SOPI model is constructed using the following forms of the threshold and density functions:

$$\begin{aligned} s_j &= \sigma_s j ; \quad j = 1, 2, \dots, J_s \\ g(s_j) &= \alpha_2 e^{-\beta_2 s_j} ; \quad j = 1, 2, \dots, J_s \end{aligned} \quad (4.5)$$

The parameters vector is thus defined as:

$$\{Q\} = [\sigma_s, \alpha_2, \beta_2]$$

The minimization problem is solved subjected to following inequality constrains on the SOPI model parameters $\alpha_2 > 0$, $\beta_2 > 0$ and $\sigma_s > 0$, while the POPI model parameters were taken as those in the previous subsection when the POPI parameters were identical to those of SOPI.

The minimization problem was solved using the MATLAB optimization toolbox under an input $v(t)=10\sin(2\pi t)$ over the interval $T=2s$ and $\Delta t=0.001$. A total of 2000 data points were considered to compute the minimization function. Solutions were attained for a number of starting values of the parameters vector, which converged to very similar parameter values. The resulting parameters of the SOPI model Γ_c , were obtained as: $\sigma_s = 0.7097$, $\alpha_2 = 0.1903$, and $\beta_2 = 0.1102$.

The SOPI model was subsequently used as a feedforward compensator for the hysteresis defined by the POPI model, Figure 4.4 illustrates the compensation of POPI model hysteresis nonlinearity using the SOPI model Γ_c . The results in the figure clearly show significantly larger reduction in the hysteresis of the output-input curves attained through composition of the two models, compared to that obtained through application of the arbitrary SOPI model (Figure 4.3).

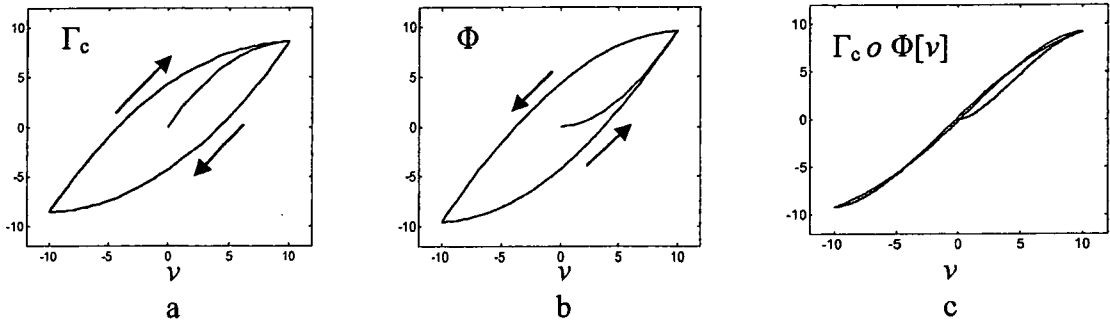


Figure 4.4: The output-input characterization of the SOPI model Γ_c , identified from the known POPI model Φ , and the compensated output under input $\nu(t)=10\sin(2\pi t)$. The hysteresis compensation effectiveness of the SOPI model as a feedforward

The hysteresis compensation effectiveness of the SOPI model as feedforward compensator is further evaluated from the error in compensated output. As an example Figure 4.5 illustrates the time histories of the percent error of the output of the POPI model (without compensation), output using the arbitrary SOPI model feedforward compensator (Figure 4.3) and the output using the identified SOPI model $\Gamma_c[\nu](t)$ Figure 4.4. The error variations are presented under the input $\nu(t)=10\sin(2\pi t)$. The results show peak position error in the order 22% in the absence of a compensator, 14% with the arbitrary SOPI model compensator and only 4% with the identified SOPI model compensator.

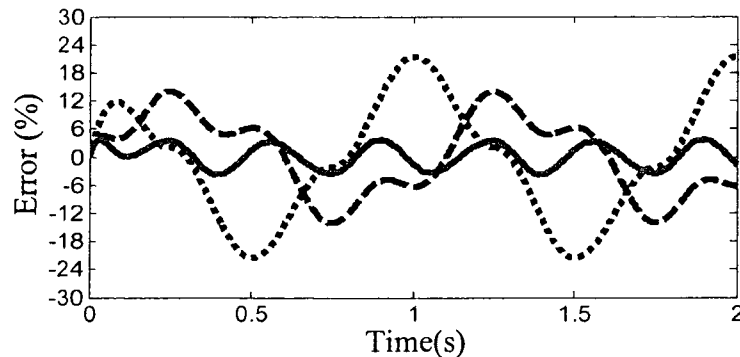


Figure 4.5: The time history of percent error in actuator displacement response with and without the SOPI model feedforward compensator: without feedforward compensator (dotted line); with arbitrary SOPI model Γ compensator (dashed line); with identified SOPI model Γ_c compensator (solid line).

This procedure can be utilized to compensate for the hysteresis nonlinearity of POPI model which has been formulated in chapter 3 to model the hysteresis of Piezoceramic actuator, this POPI model has the following parameters : $\sigma_r = 3.548$, $\alpha_1 = 0.097$, and $\beta_1 = 0.034$, according to these known POPI model parameters, the SOPI model parameters which capable to compensate this POPI model hysteresis could be identified through Equation (4.4), the SOPI model is constructed using the same forms of the threshold and density functions described in (4.5), and the minimization problem was solved using the MATLAB optimization toolbox under an input $v(t) = 5\sin(\pi t) + 35\sin(2\pi t)$ over the interval $T = 4s$ and $\Delta t = 0.005$. A total of 800 data points were considered to compute the minimization function. Solutions were attained for a number of starting values of the parameters vector, which converged to very similar parameter values. The resulting parameters of the SOPI model (Γ_c), are shown in Table 4.1, all values of threshold and density function are tabulated in Table 3.2.

The Outputs of the SOPI and POPI models were evaluated under different harmonic inputs of different frequencies and magnitudes together with compensated output to examine the effectiveness of the compensator. These included: (i) $v(t) = 40\sin(2\pi t)$; (ii) $v(t) = 40\sin(10\pi t)$; (iii) $v(t) = 15\sin(\pi t) + 25\sin(2\pi t)$; (iv) $v(t) = 5\sin(\pi t) + 35\sin(2\pi t)$; and (v) $v(t) = 20\sin(\pi t) + 20\sin(4\pi t)$. Figure 4.6 (a) through (e) illustrate the outputs of the SOPI and POPI models and the compensated output under different inputs considered in the study. The results clearly show effective mitigation of the hysteresis effects through the proposed feedforward compensator, when the SOPI model is identified from the known hysteresis nonlinearity, irrespective of the input considered. Furthermore, the SOPI model compensator can also suppress the minor

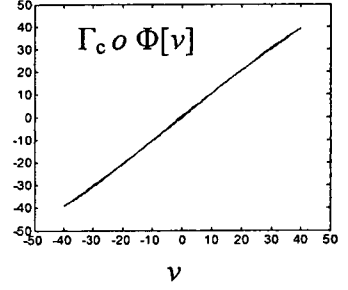
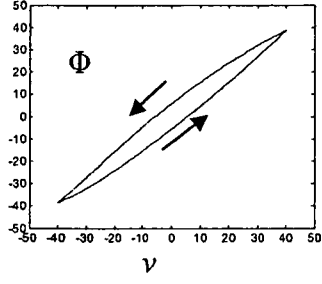
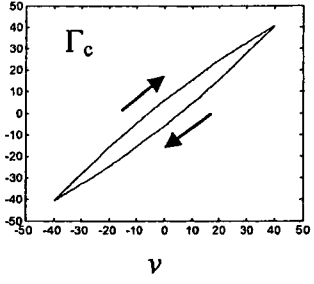
hysteresis loops obtained under the complex harmonic inputs such as $v(t)=15\sin(\pi t)+25\sin(2\pi t)$ as shown in Figure 4.6(d), $v(t)=5\sin(\pi t)+35\sin(2\pi t)$ as shown in Figure 4.6 (e) and $v(t)=20\sin(\pi t)+20\sin(4\pi t)$ as shown in Figure 4.6(f).

Table 4.1: Parameters of the Prandtl-Ishlinskii model based on the stop operator (SOPI) identified through solution of the minimization problem.

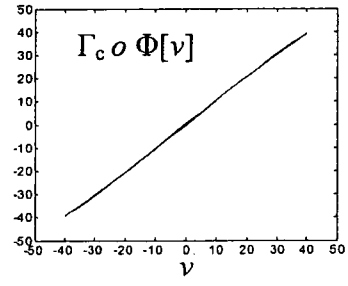
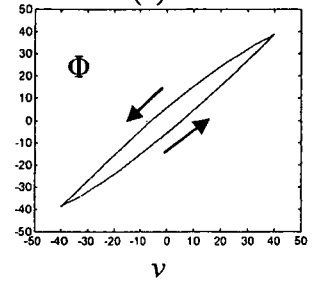
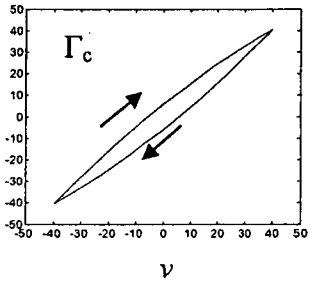
Parameter	Value
σ_s	9.8722
α_2	0.1683
β_2	0.0058

Table 4.2: The values of the thresholds and density function of the stop operator based Prandtl-Ishlinskii model.

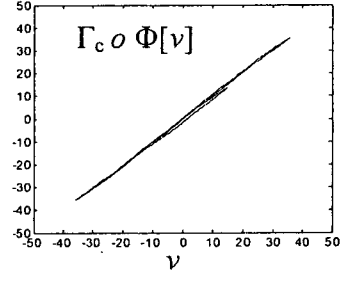
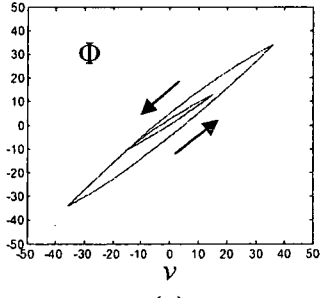
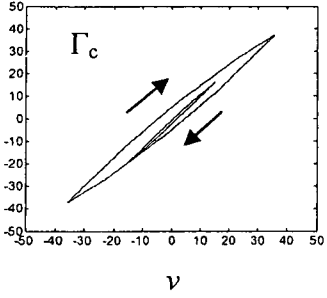
Stop operator number j	The threshold, s_j	The density function value $g(s_j)$
1	9.8722	0.1590
2	19.7444	0.1502
3	29.6166	0.1419
4	39.4888	0.1340
5	49.3610	0.1266
6	59.2332	0.1196
7	69.1054	0.1130
8	78.9776	0.1067
9	88.8498	0.1008
10	98.7220	0.0952



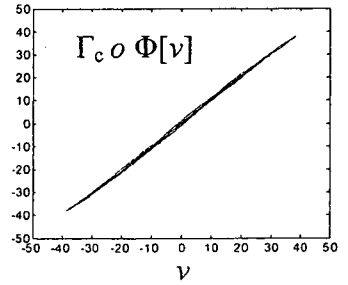
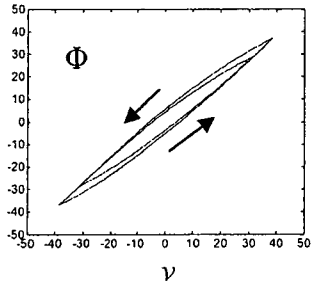
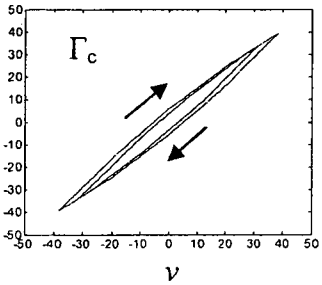
(a)



(b)



(c)



(d)

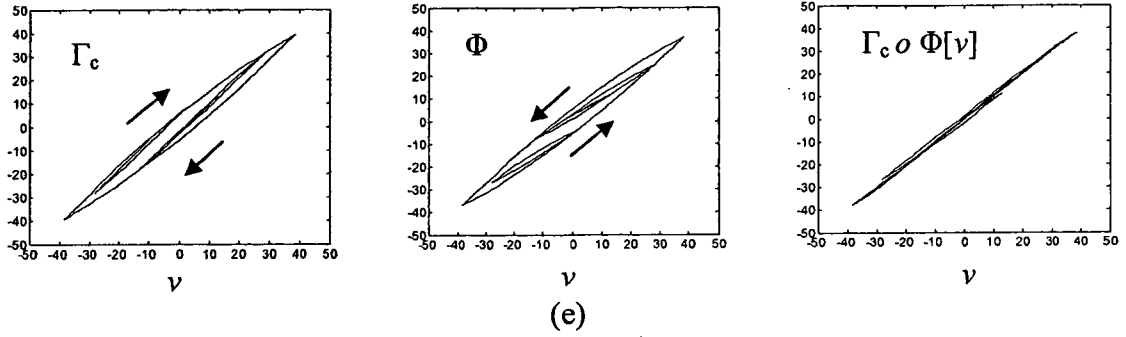


Figure 4.6: The output-input characterization of the SOPI model Γ_c , identified from the known POPI model Φ , and the compensated output under different inputs (a) $v(t)=40\sin(2\pi t)$; (b) $v(t)=40\sin(10\pi t)$; (c) $v(t)=15\sin(\pi t)+25\sin(2\pi t)$; (d) $v(t)=5\sin(\pi t)+35\sin(2\pi t)$; and (e) $v(t)=20\sin(\pi t)+20\sin(4\pi t)$.

4.4 Experimental verifications

The effectiveness of the stop operator based Prandtl-Ishlinskii model in compensating the hysteresis effects is further investigated through laboratory experiments. The experiments were performed to compensate the major and minor loops hysteresis nonlinearities of the piezoceramic actuator (P-753.31C). The measurements of the actuator displacement response were performed in the laboratory under three different excitations. These included: (i) a harmonic excitation at a low frequency of 1 Hz, $v(t)=40\sin(2\pi t)$; (ii) a harmonic excitation at a higher frequency of 5 Hz, $v(t)=40\sin(10\pi t)$; and a complex harmonic excitation, $v(t)=5\sin(\pi t)+35\sin(2\pi t)$. The first two excitations were selected to identify the compensation effectiveness of major loop output-input property of the actuator at two different frequencies, while the complex harmonic excitation was chosen to verify the compensator effectiveness for major as well as minor hysteresis loops.

The SOPI model identified from the known hysteresis nonlinearity was formulated in the SIMULINK platform. Each excitation signal was synthesized in the ControlDesk

platform and applied to the SOPI model. The output of SOPI model was subsequently applied to the input amplifier of the piezoceramic actuator through the output board and D/A. the actuator displacement response signal was then acquired in the dSpace ControlDesk using A/D together with the input signal. Figure 4.7 illustrates the schematic of the measurement setup, where the actuator hardware represents the known hysteresis and the SOPI model in SIMULINK serves as the feedforward compensator, the acquired signals were subsequently analyzed to identify, assess the SOPI model effectiveness in compensating the hysteresis in piezoceramic actuator under the selected inputs.

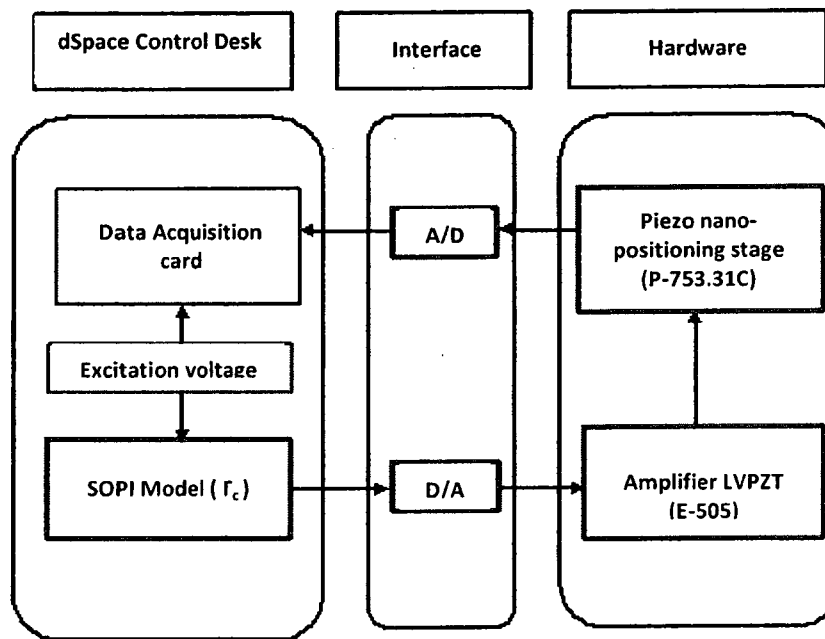


Figure 4.7: Experimental setup for compensation of hysteresis nonlinearities of the piezoceramic actuator using stop operator-based Prandtl-Ishlinskii (SOPI) model as a feed forward compensator.

The measured output-input characteristics of the piezoceramic actuator with stop operator based Prandtl-Ishlinskii model are illustrated in Figure 4.8 for the three selected inputs. The results show that the stop operator based Prandtl-Ishlinskii model can

effectively suppress the hysteresis effect, irrespective of the input applied, although some deviations are also evident. These deviations may in-part be attributed to the prediction errors of the POPI model, as seen in Figure 3.6, used to characterize the hysteresis nonlinearity and thereby define the SOPI model. The results confirm that the stop operator based Prandtl-Ishlinskii model can be effectively used as a feedforward compensator for the piezoceramic actuator.

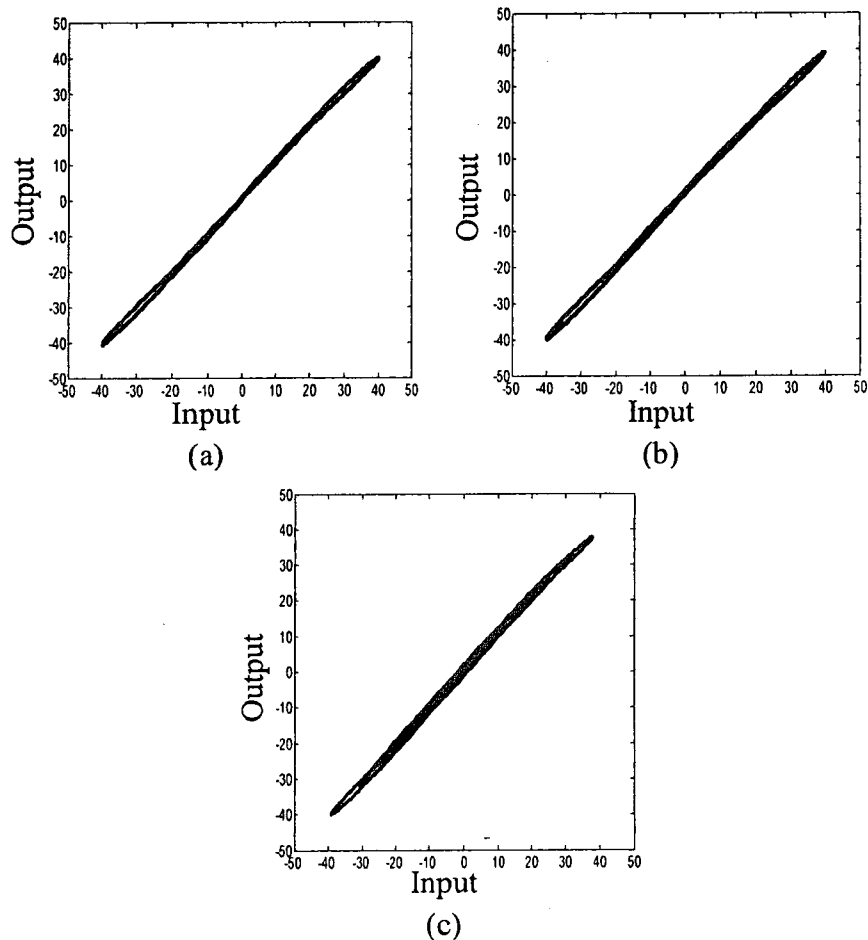


Figure 4.8: Input-output characteristics of the piezoceramic stage with SOPI model under the input: (a) $v(t)=40\sin(2\pi t)$; (b) $v(t)=40\sin(10\pi t)$; and (c) $v(t)=5\sin(\pi t)+35\sin(2\pi t)$.

The time histories of the positioning error of the piezoceramic actuator with and without the SOPI model feedforward compensator are further evaluated from both the simulation and the experimental data. The position error is expressed as a percent of the

peak position response. Figure 4.9 presents comparisons of the percent position errors with the SOPI model compensator obtained from simulations and experimental data under the selected inputs. The figure also illustrates the measured position error in the absence of the compensator. The results show peak position error in the 15-16% range, when the displacement output is measured in the absence of the compensator. The peak error in the measure responses reduces to only 4-7% when the SOPI model is implemented as the feedforward compensator, irrespective of the input considered. The corresponding simulation results show peak errors in the order of 2.5%. Table 4.3 summarizes the peak percent errors obtained from the measure data and the simulation results under the selected inputs, the results show only small differences between the error obtained from measurements and simulations.

4.5 Relations between the SOPI and POPI models

In this section essential relations between the stop and play operator-based Prandtl-Ishlinskii models are identified in order to facilitate identifications of the SOPI model parameters on the basis of a known POPI model. Furthermore, a SOPI model may be directly related to the inverse Prandtl-Ishlinskii model, which has been shown to be an effective feedforward hysteresis compensator [12, 40]. In this section, the parameters of SOPI and POPI models are evaluated to identify approximate relations between them on the basis of observed trends. The inverse of POPI model is also formulated using the proposed POPI model and compared with the proposed SOPI model.

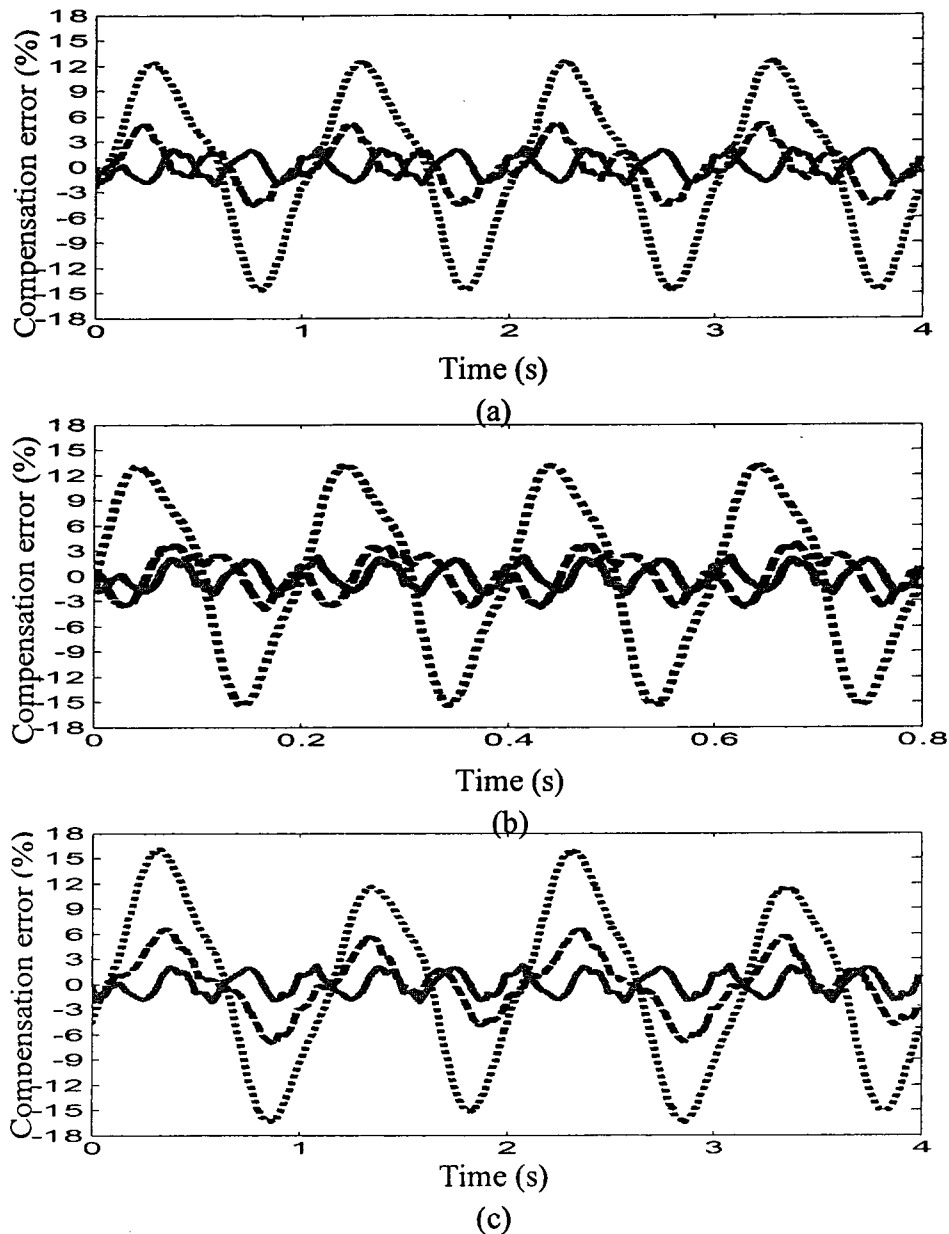


Figure 4.9: Time histories of the percent position error under different sinusoidal inputs with and without SOPI model compensator: (a) $v(t)=40\sin(2\pi t)$; (b) $v(t)=40\sin(10\pi t)$; and (c) $v(t)=5\sin(\pi t)+35\sin(2\pi t)$. (Solid line, with feedforward SOPI model compensator- simulation); (dashed line, with feedforward SOPI model compensator- experimentally); and (dotted line, without feedforward SOPI model compensator- experimentally).

Table 4.3: Peak position error (peak percent error).

	Input, $v(t)$		
	$40\sin(2\pi t)$	$40\sin(10\pi t)$	$5\sin(\pi t)+35\sin(2\pi t)$
Experimental	2.05 (5.12%)	1.57 (3.94%)	2.68 (6.7 %)
Simulation	0.90 (2.26%)	0.90 (2.26%)	1.18 (2.95%)

4.5.1 RELATIONS BETWEEN THE SOPI AND POPI MODELS

Consider the POPI model parameters, which have been identified for characterization of the hysteresis properties of the piezoceramic actuator considered in subsection 3.2.2. Further, consider the SOPI model derived on the basis of this POPI model, which was presented in section 4.3. The variations in s_j and $g(s_j)$ with r_j and $p(r_j)$, respectively, are examined to identify approximate relations. Figure 4.10 illustrates the variations in s_j and r_j , and those in $g(s_j)$ and $p(r_j)$ with considering $J_s = J_p = 10$.

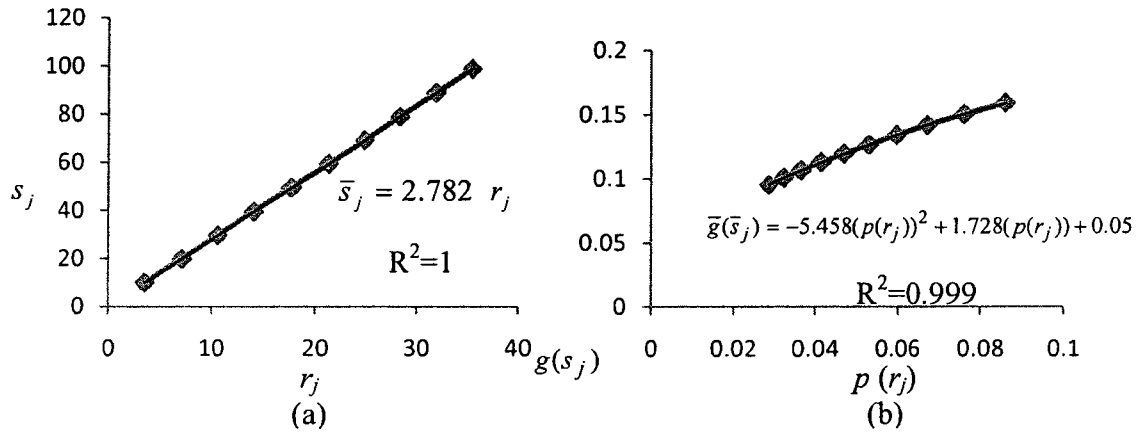


Figure 4.10: Variation in (a) the thresholds of the SOPI model with those of POPI model; and (b) the density function values of the SOPI model and those of the POPI model.

The results suggest nearly linear variations in s_j with r_j , which is attributable to the definitions of the threshold values, such that:

$$s_j = \frac{\sigma_s}{\sigma_r} r_j \quad (4.6)$$

The variations in Figure 4.10 (a) yields a linear relation ($R^2=1$) of the following form:

$$\bar{s}_j = 2.782 r_j; \quad j = 1, \dots, J_s \quad (4.7)$$

where \bar{s}_j defines the approximate threshold values of the stop operators derived from the observed variations. The constant 2.782 is identical to the ratio σ_s/σ_r . The variations in $g(s_j)$ with $p(r_j)$ can yield the following relation as appear in Figure 4.10 (b) ($R^2= 0.999$):

$$\bar{g}(\bar{s}_j) = -5.458(p(r_j))^2 + 1.728(p(r_j)) + 0.05 \quad (4.8)$$

where $\bar{g}(\bar{s}_j)$ defines the density function of the stop operator in the basis of observed variations. Using the above relations, the output of the SOPI model of a known POPI model, such that:

$$\bar{\Gamma}[v](t) = \sum_{j=1}^{J_s} \bar{g}(\bar{s}_j) E_{\bar{s}_j}[v](t) \quad (4.9)$$

Table 4.4: The thresholds and the density function values of SOPI models $\bar{\Gamma}$ and Γ_c .

j	\bar{s}_j	s_j	$\bar{g}(\bar{s}_j)$	$g(s_j)$
1	9.8727	9.8722	0.1582	0.1590
2	19.7454	19.7444	0.1500	0.1502
3	29.6181	29.6166	0.1417	0.1419
4	39.4908	39.4888	0.1337	0.1340
5	49.3635	49.3610	0.1261	0.1266
6	59.2362	59.2332	0.1189	0.1196
7	69.1088	69.1054	0.1122	0.1130
8	78.9815	78.9776	0.1061	0.1067
9	88.8542	88.8498	0.1004	0.1008
10	98.7269	98.7220	0.0951	0.0952

The SOPI model $\bar{\Gamma}$ (4.9) which has the threshold and density function values tabulated in Table 4.4, can be utilized as an effective compensator to compensate for hysteresis nonlinearity of POPI model as illustrated in Figure 4.11, the figure presents comparisons for compensation hysteresis using both SOPI models $\bar{\Gamma}$ and Γ_c under

selected input $v(t)=40\sin(2\pi t)$. Furthermore, Figure 4.12 illustrates comparisons of the percent position errors with the both models, consequently, SOPI model $\bar{\Gamma}$ which has been formulated using relations (4.7),(4.8) and (4.9) can be used as an effective compensator for hysteresis nonlinearity of POPI model.

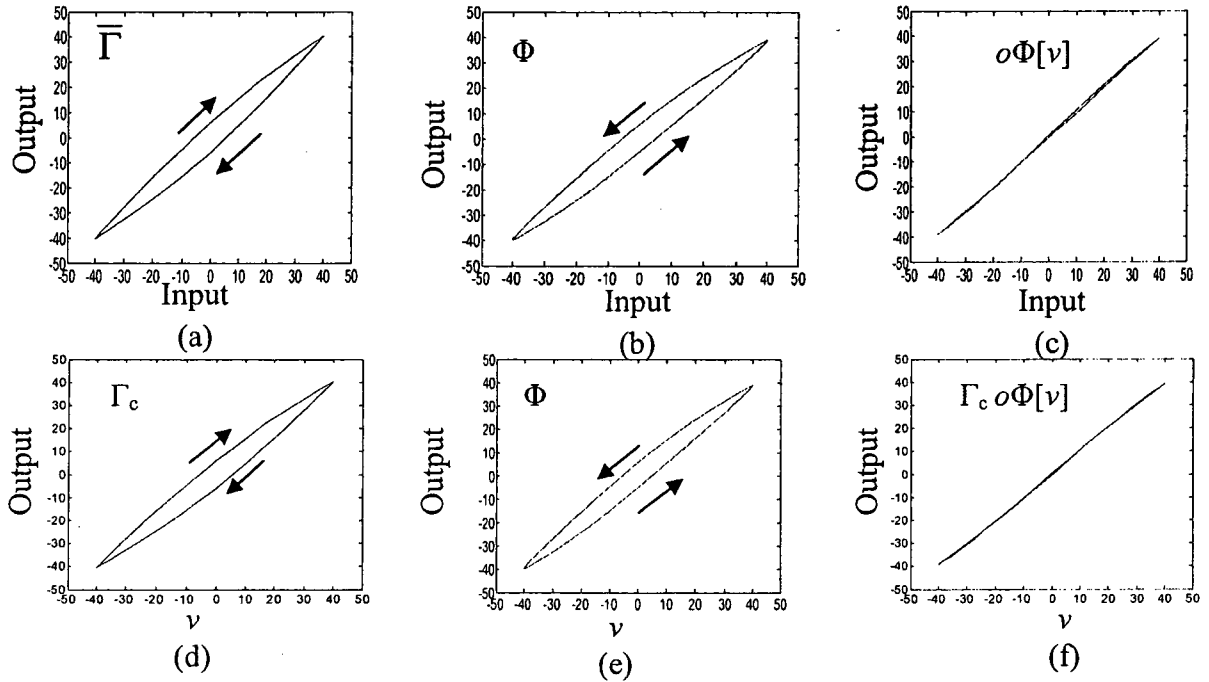


Figure 4.11 : Compensation of hysteresis nonlinearities described by a POPI model output $\Phi[v]$ presented in (b) and (e), using: (a) the SOPI model output $\bar{\Gamma}$ presented in (a), and the proposed SOPI model Γ_c model presented in (d).

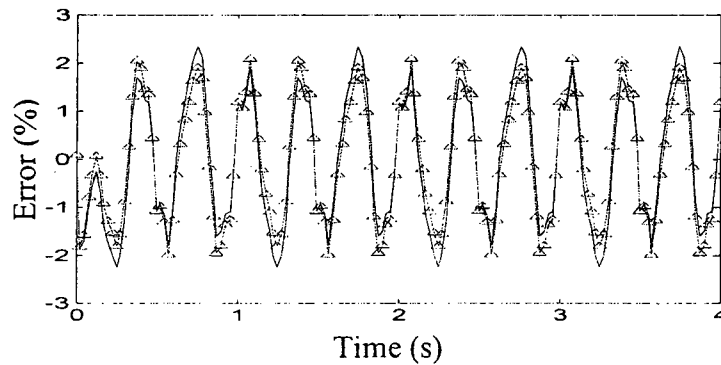


Figure 4.12: The time history of percent error of compensation error with SOPI models $\bar{\Gamma}$ and Γ_c . (——, with $\bar{\Gamma}$ model; — Δ — with Γ_c model).

4.5.2 COMPARISON OF THE INVERSE OF POPI AND SOPI MODELS

A number of studies have successfully implemented inverse hysteresis models as feedforward compensators to seek compensation of the hysteresis nonlinearities. For instance, Ge and Jouneh [7] and Song et al. [62] derived and implemented inverse Preisach models to compensate for hysteresis effects and to enhance the tracking performance of a piezoceramic actuator. Owing to the discontinuous nature of the relay operators used in the Preisach model, the inverse hysteresis model in these studies were evaluated via numerical means. Unlike the Preisach and Krasnosel'skii-Pokrovskii models, the Prandtl-Ishlinskii model offers a unique advantage, since its inverse can be obtained analytically. Krejci and Kuhnen [12] successfully applied the analytical inverse of the Prandtl-Ishlinskii model as a feedforward controller to compensate the hysteresis nonlinearities of a piezoceramic actuator. In this section, the inverse Prandtl-Ishlinskii model is briefly described and its output is compared to the proposed SOPI model, to prove the effectiveness of the SOPI model as an alternative approach for the hysteresis compensation.

The output of the inverse Prandtl-Ishlinskii model Φ^{-1} is analytically expressed as [12]:

$$\Phi^{-1}[v](t) = q^{-1}v(t) + \int_0^H p(h)F_h[v](t)dh \quad (4.10)$$

where $F_h[v]$ is the play operator of the inverse Prandtl-Ishlinskii model, and q^{-1} is a constant which is inverse of the constant q of the Prandtl-Ishlinskii model such that:

$$q^{-1} = \frac{1}{q} \quad (4.11)$$

In the inverse model, h and p_h are the threshold and the density functions, respectively, where p_h assumes a negative value. These have been related to those of the Prandtl-Ishlinskii model, r_j and $p(r_j)$, in the following manners [12]:

$$h_j = qr_j + \sum_{i=1}^{j-1} p_i(r_j - r_i) \quad (4.12)$$

$$p(h_j) = -\frac{p_j}{(q + \sum_{i=1}^j p_i)(q + \sum_{i=1}^{j-1} p_i)} \quad (4.13)$$

Using Equations (4.11), (4.12) and (4.13) the thresholds and density function values of the inverse of Prandtl-Ishlinskii model could be obtained to define the inverse model on the basis of the known POPI model. The output of the inverse Prandtl-Ishlinskii model may be obtained numerically from:

$$\Phi^{-1}[v](t) = \sum_{j=1}^{J_h} p(h_j)F_{h_j}[v](t) \quad (4.14)$$

where J_h is the number of operators used in the solution. The output of the SOPI model Γ_c obtained under an input $v(t)=40\sin(2\pi t)$ is compared with that of the inverse Prandtl-Ishlinskii model under the same input, (Figure 4.13) to illustrate the similarity in the outputs of both the models. The results show that both the models yield clockwise loops of the output-input characteristics, opposite to the direction of the observed hysteresis in the piezoceramic actuator. Furthermore, the outputs of the two models show very good agreement. The time-history of the error between the outputs of the two models is further evaluated and expressed as percent of the peak output in Figure 4.14. It

is evident that the peak error between the two models' outputs is in the order of 3%. It can thus be concluded that the proposed SOPI model is directly comparable with the analytically derived inverse of the Prandtl-Ishlinskii model.

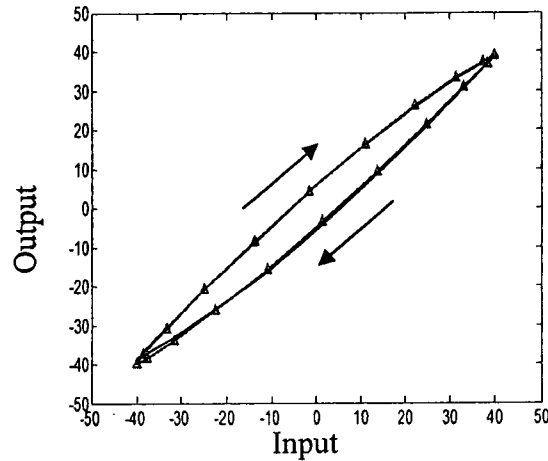


Figure 4.13: Comparison of the input-output responses of the inverse POPI Φ^{-1} and SOPI models Γ_c under a sinusoidal input: $v(t)=40\sin(2\pi t)$, (——, inverse POPI model Φ^{-1} ; —△—, SOPI model Γ_c).

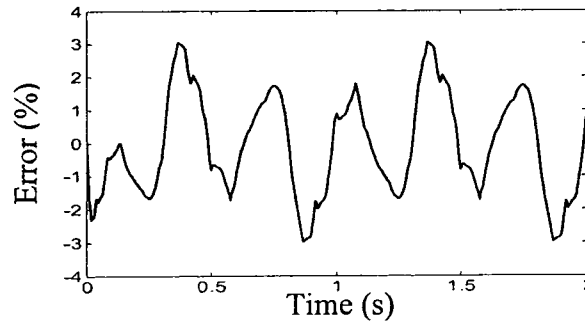


Figure 4.14: Time-history of the percent error between the inverse of POPI and the SOPI models output.

Figures 4.13 and 4.14 confirm that using SOPI model compensation effects are sit the same level comparing with the inverse of POPI model, thus it can be used as an effective alternative compensator for hysteresis nonlinearity.

4.6 Summary

The stop operator-based Prandtl-Ishlinskii model is used as a feedforward compensator for compensating model the hysteresis nonlinearity of a piezoceramic actuator. Owing to its complementary property, the hysteresis compensation effectiveness of the proposed SOPI model feedforward compensator is demonstrated through simulation examples and experimental results. In order to compensate the hysteresis effects, the parameters of the SOPI model are identified from the POPI model describing the hysteresis of the actuator. The simulation results suggest that the feedforward compensator based on the SOPI model yields nearly perfect compensation of the hysteresis nonlinearity effects. The laboratory experiment conducted to evaluate real-time compensation effectiveness of the SOPI model for a piezoceramic actuator revealed peak displacement error in the order of 5.12% for simple harmonic and for complex harmonic it was 6.7%, which was partially attributed to characterization error of the POPI model used to define the SOPI model.

Essential relations between the POPI and the SOPI models could also be identified from the observed variations in the thresholds and the density function values, and their definitions. Furthermore, the SOPI model has been verified using the inverse of POPI model: The output of the SOPI model is nearly identical to that of the inverse POPI model, while both the models exhibit hysteresis loops in the clockwise direction in the input-output curves. The peak error between the outputs of the two models was found to be in the order of 3%.

Chapter 5

Major Conclusions and Major Contributions

5.1 Major contributions

The hysteresis nonlinearities have been invariably observed in smart materials actuators such as piezoceramic and magnetostrictive actuators. Such hysteresis nonlinearities are known to cause oscillations in the responses of the open-loop systems, and poor tracking performance and potential instabilities in the closed-loop systems. This dissertation research has proposed a feedforward compensator on the basis of the stop operator-based Prandtl-Ishlinskii (SOPI) model to compensate for hysteresis nonlinearities using their complementary properties. The major contributions of this dissertation are summarized below:

- (i) A stop operator based Prandtl-Ishlinskii model has been proposed to compensate for hysteresis nonlinearities;
- (ii) The complementary properties of the stop operator based model in the relation to the play operator based model have been proven through simulations and considerations of the initial loading curves;
- (iii) The compensation effectiveness of the stop operator based Prandtl-Ishlinskii model has been demonstrated through simulations and in the laboratory for a piezoceramic actuator; and
- (iv) A methodology to identify the parameters of the SOPI model on the basis of known POPI model is proposed to facilitate the identification of the SOPI model compensator.

5.2 Major conclusions

The dissertation research has proposed a stop operator-based Prandtl-Ishlinskii model feedforward compensator for compensation of hysteresis nonlinearity in smart actuators. The conclusions drawn from the dissertation research are summarized below:

- (i) Piezoceramic actuator exhibits notable hysteresis between the input voltage and the output displacement, which is symmetric about the output. The measured input-output characteristics revealed major as well as minor hysteresis loops, while the peak position error due to hysteresis was in the order of peak error of 16% in the output of the piezoceramic actuator.
- (ii) Play operator based Prandtl-Ishlinskii (POPI) model can effectively characterize the hysteresis nonlinearity of a piezoceramic actuator between the applied voltage and the measured output displacement. The peak error in the displacement response of the model was in the order of 3.5% when compared to the measured responses under harmonic excitations at 1 and 5 Hz, and nearly 4.9% under a complex harmonic input.
- (iii) The shape function which describes the hysteresis loops of the Prandtl-Ishlinskii model was used to explore the properties of the play and stop operator-based Prandtl-Ishlinskii hysteresis loops. From the results it could be seen that the shape function of the POPI model is convex while that of the SOPI model is concave.
- (iv) The output-input characteristics of the play operator-based Prandtl-Ishlinskii model (POPI) revealed counterclockwise loops, while the stop operator-based Prandtl-Ishlinskii (SOPI) model showed clockwise hysteresis loops. Consequently, the stop operator based Prandtl-Ishlinskii (SOPI) model could be utilized to compensate the hysteresis nonlinearities of the POPI model. Compensation errors in the displacement response were approximately 2.25% under harmonic excitations at 1 and 5 Hz, and nearly 2.95% under the complex harmonic input.

- (v) The application of the SOPI model as a feedforward compensator resulted in significant reduction in the position error due to hysteresis effects, even when the SOPI model parameters are arbitrarily selected. This is attributable to the complementary properties of the stop and the play operators. Furthermore, the SOPI models shows a better effectiveness in compensating when it's parameters identified on basis of known POPI model parameters.
- (vi) The effectiveness of the proposed SOPI model compensator in real-time was further demonstrated through laboratory measurements on a piezoceramic micropositioning stage. The results showed peak position errors in the order of 6.7% under different harmonic inputs. This error is partly attributable to the characterization error of the POPI model that is used to identify the SOPI model.

5.3 Recommendations for future work

This dissertation research is considered as preliminary effort in exploring the hypothesis that the complementary properties of the stop operator-based Prandtl-Ishlinskii (SOPI) model may be applied to compensate the hysteresis nonlinearity in a smart actuator. The simulation and experimental results presented not only support the hypothesis but also demonstrate superior potential of the proposed SOPI model compensator. Far more efforts, however, are desirable to explore these potentials for real-time hysteresis compensation of a wide range of smart material actuators. Some of the recommended further efforts are listed below:

- Explore the shape function formulation in an attempt to analytically identify parameters of the stop operator-based-model.

- Explore a generalized stop operator and its properties to seek potential compensation of asymmetric hysteresis properties such as those observed in the magnetostrictive and shape memory alloy actuators.
- Attempts should be made to develop a generalized dynamic stop operator-based model using rate-dependent threshold and density functions, so as to seek hysteresis compensation at high rates of inputs.

REFERENCES

- 1 D.S. Bernstein, Ivory ghost, IEEE Control system magazine, vol.27, pp. 16-17, 2007.
- 2 D. Hughes and J. Wen, Preisach modelling of piezoceramic and shape memory alloy hysteresis, Smart Materials and Structures, vol.6, pp. 287–300, 1997.
- 3 P. Ge and M. Jouaneh, Modeling hysteresis in Piezoceramic actuators, Precision Engineering, vol. 17, pp. 211-221, 1997.
- 4 R. Smith, Smart Material System: Model Development, Society for Industrial and Applied Mathematics, 2005.
- 5 E. Shamoto and T. Moriwaki, Rigid XY _ table for ultra-precision machine tool driven by means of walking drive, Ann. CIRP, vol. 46, pp. 301–304, 1997.
- 6 X. Chen and T. Hisayama, Adaptive sliding-mode position control for piezo-actuated stage, IEEE Transactions on Industrial Electronics, vol. 55, pp. 3927 – 3934, 2008.
- 7 P. Ge and M. Jouaneh, Tracking control of a piezoceramic actuator, IEEE Transaction on Control Systems Technology, vol. 4, pp.209–216, 1996.
- 8 G. Tao and P. Kokotovic, Adaptive control of plants with unknown hysteresis, IEEE Transactions on Automatic Control, vol. 40, pp. 200-212, 1995.
- 9 R. Smith, S. Seelecke, Z. Ounais, and J. Simth, A free energy model for hysteresis in ferroelectric materials, Journal of Intelligent Materials Systems and Structures, vol. 14, pp. 719–739, 2003.
- 10 X. Tan and J. S. Baras, Modeling and control of hysteresis in Magentostriuctive actuators, Automatica, vol. 40, pp. 1469-1480, 2004.
- 11 C. Y. Su, Q. Wang, X. Chen, and S. Rakheja, Adaptive variable structure control of a class of nonlinear systems with unknown Prandtl-Ishlinskii hysteresis, IEEE Transactions on Automatic Control, vol. 50, pp. 2069 – 2074, 2005.
- 12 P. Krejci and K. Kuhnen, Inverse control of systems with hysteresis and creep, IEEE Proc Control Theory Application, vol. 148, pp. 185-192, 2001.

- 13 J. Nealis and R. Smith, Model-based robust control design for magnetostrictive transducers operating in hysteretic and nonlinear regimes, *IEEE Transactions on Control Systems Technology*, vol. 15, pp. 22-39, 2007.
- 14 R. Gorbet, Control of hysteresis systems with Preisach representations, Ph.D. dissertation, University of Waterloo, Canada, 1997.
- 15 S. Dobson, M. Noori, Z. Hou, M. Dimentberg, and T. Baber, Modeling and random vibration analysis of SDOF systems with asymmetric hysteresis, *International Journal of Non-Linear Mechanics*, vol. 32, pp. 669-680, 1997.
- 16 W. Galinaities, Two methods for modeling scalar hysteresis and their use in controlling actuators with hysteresis, Ph.D. dissertation, Dept. Math., Blacksburg, Virginia, USA, 1999.
- 17 M. Brokate and J. Sprekels, *Hysteresis and Phase Transitions*, Springer, New York, 1996.
- 18 I.D. Mayergoyz, *Mathematical Models of Hysteresis*, Elsevier, 2003.
- 19 Y. Yu, Z. Xiao, N. G. Naganathan and R.V. Dukkipati, Dynamic Preisach modelling of hysteresis for the piezoceramic actuator system, *Mechanism and Machine Theory*, vol. 37, pp. 75-89, 2002.
- 20 H. Hu, R. Ben Mrad, On the classical Preisach model for hysteresis in piezoceramic actuators, *Journal of Mechatronics*, vol. 13, pp. 85-94, 2003.
- 21 X. Tan, Control of smart actuators, Ph.D. Thesis, University of Maryland, 2004.
- 22 R. Gorbet, D. Wang and K. Morris, Preisach model identification of a two wire SMA actuator, *Proc. IEEE Int. Conf. on Robotics and Automation* 3, pp. 2161-2168, 1998.
- 23 R. Smith and Z. Ounaies, A domain wall model for hysteresis in piezoelectric materials, *Journal of Intelligent Material Systems and Structures*, vol. 11, pp. 62-79, 2000.
- 24 J.W. Macki, P. Nistri, and P. Zecca, Mathematical models for hysteresis, *SIAM Review*, vol.35, pp. 94-123, 1993.
- 25 A. Visintin, *Differential models of hysteresis*, Spring-Verlag, Berlin, Hiedelberg, 1994.

- 26 G. Bertotti, Dynamic generalization of the scalar Preisach model of hysteresis, *IEEE Transactions on Magnetics*, vol. 28, pp. 2599–2601, 1992.
- 27 L. Grcev, Z. Tasev, and L. Kocarev, Frequency dependent model of ferromagnetic hysteresis for time domain analysis of cable shields, *IEEE International Symposium on Electromagnetic*, pp. 586–591, 1997.
- 28 M. Krasnoselskii and A. Pokrovskii, *Systems with Hysteresis*, 1983; Springer, Moscow, 1989.
- 29 I.D. Mayergoyz, G Friedman, and C. Salling, Comparison of the classical and generalized Preisach hysteresis models with experiments, *IEEE Transactions on Magnetics*, vol. 25, pp. 3925–3927, 1998.
- 30 Kyoung Kwan Ahn and Nguyen Bao Khan, Modeling and control of shape memory alloy actuators using Preisach model, genetic algorithm and fuzzy logic, *Mechatronics*, vol. 18, pp. 141-152, 2008.
- 31 Y. Ni, J. Ko and C. Wong, Identification of nonlinear hysteresis isolator from periodic vibration tests , *Journal of Sound and Vibration* , 1998.
- 32 H.T. Banks, A.J. Kurdila and G. Webb. Identification of hysteretic control influence operators representing smart actuators, *Mathematical problems in engineering*, vol.3, pp. 287-328, 1997.
- 33 P. Ge, *Modeling and Control of Hysteresis in Piezoceramic actuator*, Ph.D. Thesis, University of Rhode Island, 1996.
- 34 M. Krasnoselskii and A. Pokrovskii, *Systems with hysteresis*, Nauka, Moscow 1983; Springer-Verlag, 1989.
- 35 H. Janocha and K. Kuhnen, Real-time compensation of hysteresis and creep in piezoelectric actuators, *Sensors and Actuators A: Physical*, vol. 79, pp. 83-89, 2000.
- 36 H. Liaw; B. Shirinzadeh and J. Smith, Sliding-mode enhanced adaptive motion tracking control of piezoelectric actuation systems for micro/Nano Manipulation, *IEEE Transactions on Control Systems Technology*, vol. 16, pp. 826-833, 2008.
- 37 Xiaobo Tan, John S. Baras, P.S. Krishnaprasad, Control of hysteresis in smart actuators with application to micro-positioning, *Systems & Control Letters*, vol. 54, pp. 483 – 492, 2005.

- 38 H.J. Pahk, D.S. Lee and J.H. Park, Ultra precision positioning system for servo motor–piezo actuator using the dual servo loop and digital filter implementation, *International Journal of Machine Tools & Manufacture*, vol. 41, pp. 51-63, 2001.
- 39 M. Al Janaideh, S. Rakheja, and C-Y. Su, A generalized Prandtl-Ishlinskii model for characterizing hysteresis nonlinearities of smart actuators, *Smart Materials and Structures*, vol. 18, pp.1-9, 2009.
- 40 M. Al Janaideh, Chun-Yi Su and Subhash Rakheja, An analytical generalized Prandtl-Ishlinskii model inversion for hysteresis compensation in micro-positioning control, submitted for publication in *IEEE/ASME Transactions on Mechatronics systems*.
- 41 S. Gonda, T. Doi, T. Kurosawa, Y. Tanimura, N. Hisata, T. Yamagishi, H. Fujimoto, and H. Yukawa, Accurate topographic images using a measuring atomic force microscope, *Appl. Surface Sci.*, vol. 144–145, pp. 505–509, 1999.
- 42 D. Song and C. J. Li, Modeling of piezo actuator’s nonlinear and frequency dependent dynamics, *Mechatronics*, vol. 9, pp. 391–410, 1999.
- 43 M. Goldfarb and N. Celanovic, Modeling piezoelectric stack actuators for control of micromanipulation, *IEEE Transactions on Control Systems Technology*, vol. 17, pp. 69–79, 1997.
- 44 P. Ge and M. Jouaneh, Generalized Preisach model for hysteresis nonlinearity of piezoceramic actuators, *Precision Engineering*, 1997.
- 45 J. H. Park, K. Yoshida, and S. Yokoto, Resonantly driven piezoelectric micropump: Fabrication of a micropump having high power density, *Mechatronics*, vol. 9, pp. 687–702, 1999.
- 46 S. Böhm, W. Olthuis, and P. Bergveld, A plastic micropump constructed with conventional techniques and materials, *Sensors and Actuators*, vol. 77, pp. 223–228, 1999.
- 47 K. Ikuta, M. Tsukamoto and S. Hirose, Mathematical model and experimental verification of shape memory alloy for designing micro actuator, *Proc. IEEE Int. Conf. on Micro Electro Mechanical Systems*, pp. 103–111, 1991.
- 48 W. Ang, F. Garmon, P. Khosla, and C. Riviere, Modeling rate-dependent hysteresis in piezoelectric actuators, in *Proc. International Conf. of Intelligent Robots and Systems*, Lasvegas, Nevada, pp. 1975–1980, 2003.
- 49 J. Kim and S. Nam, Development of a micro-depth control system for an ultra-precision lathe using a piezo-electric actuator, *International Journal of Machine*

- Tools and Manufacture, vol. 37, pp. 495-509, 1997.
- 50 K. H. Park, J. H. Lee, S. H. Kim, and Y. K. Kwak, High speed micro positioning system based on coarse/fine pair control, *Mechatronics*, vol. 5, no. 6, pp. 645–663, 1995.
 - 51 M. Sasaki, T. Suzuki, E. Ida, F. Fujisawa, M. Kobayashi, and H. Hiria, Track-following control of a dual-stage hard disk drive using a neurocontrol system, *Engineering Applications of Artificial Intelligence*, vol. 11, pp. 707–716, 1998.
 - 52 J. Kim and S. Nam, Development of a micro-positioning grinding table using piezoelectric voltage feedback, *Institution of Mechanical Engineers, proceedings of the Part B-Journal of Engineering Manufacture* , vol. 209, pp. 469-474, 1995.
 - 53 B. Zhang and Z. Zhu, Developing a linear piezomotor with nanometer resolution and high stiffness, *IEEE/ASME Trans. Mechatronics*, vol. 2, pp. 22–29, 1997.
 - 54 R. Dong, Y. Tan, H. Chen and Y. Xie, A neural networks based model for rate-dependent hysteresis for piezoceramic actuators, *Sensors and actuators*, vol.143, pp. 370-376, 2008.
 - 55 H. Haitjema, Dynamic probe calibration in the limm region with nanometer accuracy, *Precision Eng.* , vol. 19, pp. 98–104, 1996.
 - 56 D. R. Meldrum, A biomechatronic fluid-sample-handling system for DNA processing, *Mechatronics*, vol. 2, pp. 99–109, 1997.
 - 57 Y.Q. Ni, J.M. Ko, and C.W. Wong, Identification of nonlinear hysteretic isolators from periodic vibration tests, *journal of sound and vibration*, vol. 217, pp.737-756, 1998.
 - 58 Tsai Chen, Robust tracking control of a Piezoactuator using a new approximate hysteresis model, *Journal of Dynamic Systems, Measurement and Control*, 2003.
 - 59 S. Lee, T. Royston and G. Friedman, Modeling and compensation of hysteresis in piezoceramic transducers for vibration control, vol. 11, pp. 781-789, 2008.
 - 60 C.Y. Su, Y. Stepanenko, J. Svoboda and T.P. Leung, Robust adaptive control of a class of nonlinear systems with unknown backlash-like hysteresis ,*IEEE Tranactions on Automatic Control*, vol.45, pp. 200-212, 2000.
 - 61 I.D. Mayergoyz and G. Friedman, Generalized Preisach model of hysteresis, *IEEE Transactions on Magnetics*, vol. 24, pp. 212 – 217, 1998.

- 62 G. Song, J Zhao, X. Zhou, and J.Abreu-Garcia, Tracking control of a piezoceramic actuator with hysteresis compensation using inverse Preisach model, IEEE/ASME Transaction on Mechatronics, vol. 10, pp.198-209, 2005.
- 63 S. Yingfeng and K. Leang , Repetitive control with Prandtl-Ishlinskii hysteresis inverse for piezo-based nanopositioning, in Proc. of the 2009 American Control Conference, pp. 301 - 306, 2009.

Appendix A

The mathematical proof of complementary property

This appendix summarizes the proof of the complementary property of the stop and play operators using two different approaches. The first approach considers the play operator to derive a relation with the stop operator, while the second approach utilizes the stop operator formulation to derive a relation with the play operator.

Approach I

Consider the play operator defined in (2.13):

$$f_r(v, z) = \max\{v - r, \min\{v + r, z\}\} \quad (\text{A.1})$$

The above relation could be rewritten as:

$$v - f_r(v, z) = v - \max\{v - r, \min\{v + r, z\}\} \quad (\text{A.2})$$

The order of minima and maxima may be attained to yield

$$v - f_r(v, z) = v + \min\{-(v - r), \max\{-(v + r), -(z)\}\} \quad (\text{A.3})$$

which may be further simplified to:

$$v - f_r(v, z) = v + \min\{r - v, \max\{-v - r, -z\}\} \quad (\text{A.4})$$

The right-hand side of the above equation can be rewritten as:

$$v - f_r(v, z) = \min\{(r - v) + v, \max\{(-v - r) + v, (-z) + v\}\} \quad (\text{A.5})$$

The above equation further reduces to:

$$v - f_r(v, z) \min\{r, \max\{-r, v - z\}\} \quad (\text{A.6})$$

From the definition of the stop operator, in (2.8) and $r=s$, the relationship between the play and stop operator is obtained as:

$$v - f_r(v, z) = e_r(v - z) \quad (\text{A.7})$$

Approach II

Consider the stop operator defined in (2.13):

$$e_s(v) = \min\{\max\{s, v\}, s\} \quad (\text{A.8})$$

For complementary property $s=r$, the above equation could be rewritten as:

$$v(t) - e_r(v) = v(t) - \min\{\max\{-r, v(t) - v(t_i) + E(t_i)\}, r\} \quad (\text{A.9})$$

The order of minima and maxima may be attained to yield:

$$v(t) - e_r(v) = v(t) + \max\{r, \min\{-r, -(v(t) - v(t_i) + E(t_i))\}\} \quad (\text{A.10})$$

Which may be further simplified to:

$$v(t) - e_r(v) = v(t) + \max\{r, \min\{-r, -v(t) + v(t_i) + E(t_i)\}\} \quad (\text{A.11})$$

The right-hand side of the above equation can be rewritten as:

$$v(t) - e_r(t) = \max\{v(t) - r, \min\{v(t) + r, v(t_i) + E(t_i)\}\} \quad (\text{A.12})$$

$$v - e_r(v) = f_r(v, v(t_i) + E(t_i)) \quad (\text{A.13})$$